HYDROLOGICAL PROCESSES
Hydrol. Process. **14**, 1017–1044 (2000)

Development and application of a spatially-distributed Arctic hydrological and thermal process model (ARHYTHM)

Ziya Zhang, Douglas L. Kane* and Larry D. Hinzman
Water and Environmental Research Center, University of Alaska Fairbanks, Fairbanks, AK 99775, USA

Abstract:

A process-based, spatially distributed hydrological model was developed to quantitatively simulate the energy and mass transfer processes and their interactions within arctic regions (*ar*ctic *hy*drological and *th*ermal *m*odel, ARHYTHM). The model first determines the flow direction in each element, the channel drainage network and the drainage area based upon the digital elevation data. Then it simulates various physical processes: including snow ablation, subsurface flow, overland flow and channel flow routing, soil thawing and evapotranspiration. The kinematic wave method is used for conducting overland flow and channel flow routing. The subsurface flow is simulated using the Darcian approach. The energy balance scheme was the primary approach used in energy-related process simulations (snowmelt and evapotranspiration), although there are options to model snowmelt by the degree-day method and evapotranspiration by the Priestley–Taylor equation. This hydrological model simulates the dynamic interactions of each of these processes and can predict spatially distributed snowmelt, soil moisture and evapotranspiration over a watershed at each time step as well as discharge in any specified channel(s). The model was applied to Imnavait watershed (about 2·2 km^2) and the Upper Kuparuk River basin (about 146 km^2) in northern Alaska. Simulated results of spatially distributed soil moisture content, discharge at gauging stations, snowpack ablations curves and other results yield reasonable agreement, both spatially and temporally, with available data sets such as SAR imagery-generated soil moisture data and field measurements of snowpack ablation, and discharge data at selected points. The initial timing of simulated discharge does not compare well with the measured data during snowmelt periods mainly because the effect of snow damming on runoff was not considered in the model. Results from the application of this model demonstrate that spatially distributed models have the potential for improving our understanding of hydrology for certain settings. Finally, a critical component that led to the performance of this modelling is the coupling of the mass and energy processes. Copyright © 2000 John Wiley & Sons, Ltd.

KEY WORDS spatially distributed hydrological model; arctic; soil moisture; snowmelt; evapotranspiration; streamflow; overland flow; subsurface flow; digital elevation model; permafrost; tundra

INTRODUCTION

The arctic ecosystem (defined here as an area of continuous permafrost) differs from those in more temperate regions, primarily because of the cold temperatures, dominance of snow cover and large annual variation in solar radiation. Past interests in hydrological processes in arctic regions were driven primarily by resource

* Correspondence to: D. L. Kane, University of Alaska, Water and Environmental Research Center, Institute of Northern Engineering, 460 Duckering Building, Fairbanks, AK 99775-5860, USA. E-mail: ffdlk@uaf.edu

Contract/grant sponsors: Arctic System Science (ARCSS) Land Atmosphere Ice Interactions (LAII) Program, US National Science Foundation.
Contract/grant numbers: OPP-9214927 and OPP-9318535.

Received 8 September 1997
Accepted 2 April 1999

development; however, hydrological research is currently being conducted for numerous other reasons. It is broadly acknowledged that arctic regions play an important role in Earth's climate dynamics (Alley, 1995). It also represents potentially important sources and/or sinks of greenhouse gases. A changing climate could in turn induce numerous biological and physical changes that could augment or retard global climate change and significantly impact arctic ecosystems (Rouse *et al*., 1997). Also, arctic environments are fragile systems that are relatively sensitive to anthropogenic impact and climate change (Roots, 1989; Kane *et al*., 1991b; Crawford, 1997; Rouse *et al*., 1997). Advancing our understanding of the hydrology of this region can be accomplished by coupled field and modelling studies. Reported here is the development and application of an *ar*ctic *hy*drological and *th*ermal *m*odel (ARHYTHM).

Understanding coupled hydrological and thermal processes is essential when studying regional and global climatic change and its consequences. As a main linkage between atmospheric and terrestrial/aquatic systems, hydrological processes are very important and yet complex. To quantify the interactive dynamics of the arctic system, a process-based and spatially distributed hydrological model that covers all of the important aspects of the water and energy balances and their interactions is needed. Such a process-based, spatially distributed hydrological model offers several advantages (Goodrich, 1990; Woolhiser *et al*., 1990; Wigmosta *et al*., 1994; Beven, 1996) over lumped conceptual or empirical models. First, it provides greater amounts of detailed information over the entire basin, rather than just lumped basin averages. Second, its spatially distributed output data can be very useful when the model is coupled to other spatially distributed models such as those for chemical and biological processes.

There are several hydrological models that have the ability to simulate spatial variation of physical processes: such as the SHE model (Systéme Hydrologique Européen) (Jonch-Clausen, 1979; Abbott *et al*., 1986) and the TOPMODEL (Beven and Kirkby, 1979). Kite (1978, 1989) developed a simple lumped reservoir parametric (SLURP) model to simulate hydrological responses of watersheds. Later, Kite and Kouwen (1992) improved the same model by computing the rainfall–runoff and snowmelt processes separately for different land cover classes. By relating the model parameters to vegetation type, Kite (1993) used a similar model, SLURP_GRU, to study the climate change and produce more realistic estimates of the resulting changes in streamflow. Kite *et al*. (1994) also combined a hydrological model with a GCM for a macroscale watershed. Wigmosta *et al*. (1994) presented a distributed hydrology–vegetation model that includes canopy interception, evaporation, transpiration, and snow accumulation and melting, as well as runoff generation via the saturation excess mechanisms. The model was applied to a basin of 2900 km^2 in north-western Montana. Jackson *et al*. (1996) developed a spatially distributed hydrological model to simulate the snowmelt-driven hydrological response of a small arid mountain watershed. Snow accumulation and drifting, evapotranspiration and subsurface mass balance were included. Each of the above models was generally developed for a specific application to a particular climate and hydrological regime at a defined watershed scale. Therefore, each one emphasizes those hydrological processes that are important in light of the problem studied, climate and scale of interest. Some of these models either deal with only some elements of the hydrological cycle or the simulation period is for a short length of time, such as one storm event. Others deal with processes in temperate climates that have a different hydrological regime than the Arctic. Regardless, all of these models require a substantial set of good quality data to produce useful simulations.

In the Arctic, snow accumulation, redistribution of snow by wind and snow ablation are important hydrological events each year. The continuous permafrost acts like an impermeable layer for groundwater flow, restricting subsurface flow within the shallow active layer (the shallow soil layer above permafrost that experiences freeze and thaw every year). The soil thermal and hydraulic properties change throughout the year because of the thawing and freezing or with changing moisture content. Long, cold winters and short summers with low precipitation and low temperatures characterize this harsh environment. These special characteristics of the Arctic must be studied and quantified before they may be simulated adequately. Complementary studies have been ongoing in various watersheds of Kuparuk River on the North Slope of Alaska since 1985 (Kane *et al*., 1989, 1990, 1991a, 1993; Hinzman and Kane, 1991; Hinzman *et al*., 1991a,b, 1993a,b; Kane and Hinzman, 1993; McNamara *et al*., 1997, 1998). These studies cover many aspects of

hydrological processes required for a basic understanding of arctic hydrology, including data collection, analyses and modelling to simulate various processes and their interrelationships. Many studies of mass and energy transfers in the Canadian Arctic have contributed a great deal to our present understanding of arctic hydrology (Marsh and Woo, 1979; Woo and Sauriol, 1980; Woo, 1982, 1983, 1986; Woo and Heron, 1987; Rouse *et al*., 1997). Many other researchers have contributed to our understanding of arctic meteorological processes (Weller and Holmgren, 1974; Benson, 1982; Clagett, 1988). This model was developed from the rigorous field research and analyses of these and other investigators.

Currently, most simulations of arctic hydrology rely on lumped parameter models, which produce averaged results that reflect the total/average response of a watershed. Most of these model applications were carried out in small watersheds where the assumption of uniformity is more realistic. Spatially distributed models that use distributed input such as precipitation can be utilized to study spatial variability of hydrological processes. This type of model has not, until now, been available for the Arctic. Here we will describe the development of such a model and outline how it can be applied to study detailed hydrological and energy processes within arctic basins (basins with continuous permafrost). Our primary objective was to develop a tool for the spatial prediction of soil moisture. Results from the application of this model to two watersheds, Imnavait Creek and the Upper Kuparuk River basin, located at the North Slope of Alaska are presented and discussed.

MODEL DEVELOPMENT

This model is comprised of two parts, one that simulates the drainage of the basin and one that simulates hydrological processes. Initially the drainage simulation is run once and does not change for a basin, whereas the process simulations change as the initial conditions and state variables change and/or the parameters change.

Topographic delineation of a watershed

Hydrological response of a watershed is influenced by many interacting factors, primary among which is topography. There are many articles that discuss the effect of topography on some aspects of hydrological processes (Beven and Wood, 1983; Palacios and Cuevas, 1986; Silfer *et al*., 1987; Gary and Sen, 1994; Wolock and Price, 1994). The watershed topography serves as an important factor in determining the streamflow response of a basin to precipitation because it controls the movement of water within the basin. It also affects the spatial distribution within the watershed of fluxes such as surface and subsurface water, sediment and dissolved chemicals. It is essential to correctly depict slope, aspect and drainage characteristics of a watershed for use in spatially distributed models.

Basic unit/element of watershed. Generally, terrain surfaces may be represented by a series of discrete points, which are characterized by x, y, and z coordinates. Triangular and rectangular elements are often used as the basic uniform areas for mass and energy balances when conducting hydrological modelling (Silfer *et al*., 1987; James and Kim, 1990; Jones *et al*., 1990; Paniconi and Wood, 1993; Gary and Sen, 1994). Node-based models are also used (Wigmosta *et al*., 1994). In our model, similar to the work by Silfer *et al*. (1987), a triangular element scheme (Figure 1a) is used to represent the watershed. Utilization of triangle elements has certain advantages over other types of elements (Jones *et al*., 1990). Triangle elements conform more nearly to the three-dimensional geometry of an irregular watershed. It is more efficient to calculate the water flow directions using triangular elements, as opposed to rectangular elements, because it is possible to fit a plane through the three points of the triangle whereas a rectangle must be fit with a non-planar surface. Having created a basic unit area, we can calculate flow area, slope, drainage networks, ridges, drainage area and other related information needed when conducting physical simulations. It should be noted that the elements can be based upon a regularly or irregularly spaced grid.

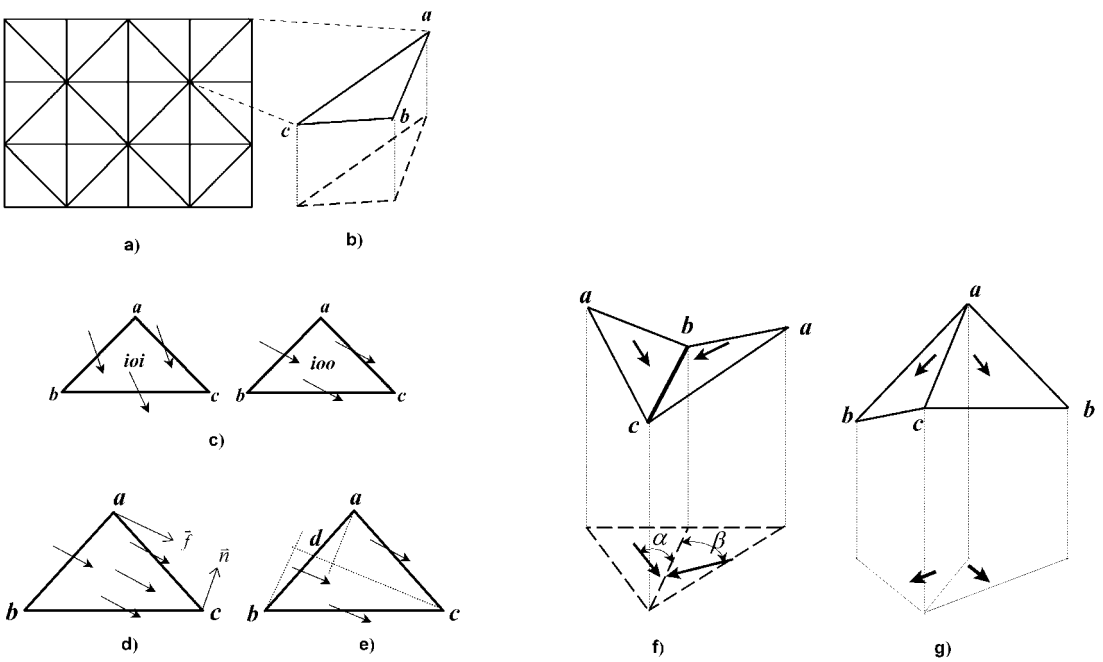

Figure 1. (a) Triangular elements used in the model, (b) node notation, (c) two possible flow cases for each element, (d) flow direction, (e) partitioning of flow through element boundaries, (f) flow pattern for channel segments, (g) ridge (watershed) divides

Flow directions and channel networks. Flow direction needs to be determined for subsurface flow, overland flow and channel flow. Flow direction is calculated before conducting any flow routing. The flow direction is assumed to be the same for subsurface and overland flow for each element. This is based on the effect permafrost has on subsurface flow in the active layer. The determination of flow direction within each element is based on its gradient. For each element (Figure 1b), the three nodes are identified as *a*, *b*, and *c*, which refer to the point at the highest, middle, and lowest elevation, respectively. Two letters are used to indicate whether flow is leaving (*o*) or entering (*i*) the element through its boundaries. So for any case, two combinations of *i* and *o* can represent the flow patterns. For example, *ioi* means water flows into the element through boundaries $\overline{ab}$ and $\overline{ac}$ flows out through boundary $\overline{bc}$. Figure 1c shows two possible flow cases, which are *ioi* and *ioo*. Note that the flow is always into the element through the boundary $\overline{ab}$ because *a* and *b* are the highest two points among the three nodes and always out of the element through the boundary $\overline{bc}$ because *b* and *c* are the lowest two points among the three nodes. By calculating the normal of the cross-product of the vectors from the lowest vertex, $\vec{\mathbf{n}} = \overline{bc} \times \overline{ac}$, the gradient of the plane can be determined. Then the flow direction ($\vec{\mathbf{f}}$) is known for each element (Figure 1d), assuming that flow within each element is parallel to its plane gradient. In the case of *ioo* (Figure 1e), the partitioning of the areas that contribute flow through $\overline{bc}$ and $\overline{ac}$ are the triangular areas of *bcd* and *adc* respectively, where *d* is the interception of $\overline{ab}$ and $\overline{cd}$, which is parallel to flow direction $\vec{\mathbf{f}}$. Once the flow direction of each element is determined, it is assumed not to change with time.

Channel segments can then be determined based on the flow direction in every element. If two elements share a common outflow boundary (Figure 1f), then that common boundary is considered a channel reach. It is possible that the downstream reach of the created channel segment may not be a channel based on the condition described above; however, once a channel reach is initiated, that channel is continued until it meets another channel or reaches the boundary of the watershed. This can be accomplished by accepting the fact that the flow will follow the steepest path among the possible boundaries. Similar concepts can be applied to

find ridges. If two adjacent elements share a common inflow boundary (flow pattern *i*), then that boundary becomes a single ridge segment (Figure 1g). Ridges defining the watershed boundary will be continuous, but not ridges internal to the watershed.

Flat area considerations. Flow direction determination in flat areas needs special consideration (Lee and Schacter, 1980; Petrie and Kennie, 1987; Jones *et al*., 1990). The method used to determine flow direction for a non-flat element does not work mathematically for a flat element. Physically, however, owing to water accumulation, water is moving across flat areas. So, the direction must be established before conducting flow routing. In our model, water will generally flow from higher elevations to lower elevations by flooding flat areas. So, for each flat element, the elevations at the nodes are temporarily replaced by a new set of data that is generated by averaging the elevation values of its surrounding nodes. Once the directions are determined, the elevation values for those flat elements are set back to the original ones. During flow calculations, water may accumulate in a flat channel or element until a hydraulic gradient is created.

Simulations of physical processes

Although many processes are similar, arctic hydrologic systems have several unique characteristics, such as the existence of permafrost and a dynamic active layer, that create a spatial domain with a constantly changing lower boundary. In the model described here, all of the important components shown in Figure 2 have been considered. Some processes, however, have not been fully incorporated in these simulations as physically based or spatially distributed. Coupling an energy balance thermal model with the simulated soil moisture distribution to accurately consider changing thermal properties associated with conductive heat transfer, for example, should be incorporated to solve the soil thawing/freezing. In the simulations of the model described here, however, a simple function of air temperature (degree-hour method) is used to estimate the soil depth of thaw. In our effort to accurately and completely model arctic hydrological processes, we develop a model of surface and subsurface heat transfer processes across the same spatial and temporal domain (Hinzman *et al*., 1998). Following is a discussion of each hydrological process that results in a mass flux and the relevant energy fluxes.

Snowmelt. Snowmelt is a major component of the hydrological cycle in the Arctic. So, correctly simulating snowmelt and predicting subsequent runoff from the watershed are important components of arctic hydrological modelling. The annual snow cycle is characterized by a relatively long accumulation period of eight to nine months, followed by a short melt season (van Everdingen, 1987; Kane *et al*., 1997). We initiate hydrological simulation at the end of winter, prior to snowmelt, so it is not necessary to model accumulation or redistribution of snow, it is only necessary to consider the end of winter snowpack distribution. In the foothills of the Brooks Range, the snow melts in a relatively short period (about 10 to 14 days) and usually generates the highest stream flows of the year. Current snowmelt models generally use the energy balance method or a simple temperature index method, depending on what kind of data are available and what results are needed (Laramie and Schaake, 1972; Price and Dunne, 1976; Bergström, 1986; Hinzman *et al*., 1991; Hinzman and Kane, 1991; Kane *et al*., 1993, 1997; Wigmosta *et al*., 1994). In our model, the surface

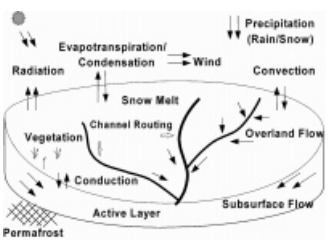

Figure 2. Hydrological and thermal processes simulated for every element within an arctic watershed

energy balance method has been used. A simpler degree-day method also has been included as an option because in many areas too little data are available to do an adequate surface energy balance.

Energy balance method. The energy balance of the snowpack is a physically based approach that considers the important heat transfer processes occurring on the surface of the snowpack, including heat storage within the snowpack. It can be expressed as:

$$Q_m = Q_{net} + Q_h + Q_e + Q_a + Q_c - Q_{cc} \quad (1)$$

where Q_m (W/m^2) is the energy utilized for melting the snowpack when it is positive; Q_{net} (W/m^2) is net radiation energy, either measured by a net radiometer or calculated as the sum of individual incoming and outgoing long and short wave fluxes; Q_h (W/m^2) is sensible heat flux resulting from turbulent convection between the watershed snow surface and the air; Q_e (W/m^2) is latent heat flux associated with evaporation/sublimation and condensation; Q_a (W/m^2) is the energy advected by moving water (i.e. rainfall); Q_c (W/m^2) is the energy flux via conduction from the snow to the soil and is neglected because the vertical temperature gradient during melting is relatively small; Q_{cc} (W/m^2) is the cold content of the snowpack, which is defined as the amount of heat needed to bring the snowpack to a ripe condition prior to melt or the amount of energy that may be released in cooling or refreezing of liquid water in the snow during extended cold periods (Bengtsson, 1984). This energy deficit or cold content that accumulates when the melt is interrupted by cold weather must be satisfied prior to resumption of snowmelt. If Q_m in Equation (1) is negative, it means that the combined energy of $Q_{net} + Q_h + Q_e + Q_a + Q_c$ is not enough to overcome the cold content (Q_{cc}). This indicates that if there is liquid water within the snowpack, it will freeze or if no liquid water is present, the snowpack will cool further. This is typical on nights when the air temperature drops below freezing or when snowmelt is interrupted for days by a cold period.

Sensible and latent heat fluxes to and from the surface of the snowpack are calculated using an aerodynamic approach. This approach takes into account turbulent transfer mechanisms and vertical gradients of temperature and vapour pressure in order to obtain sensible (Q_h) and latent heat (Q_e) fluxes (Moore, 1983):

$$Q_h = \rho_a \cdot C_{pa} \cdot K_h \cdot dT/dz = \rho \cdot C_{pa} \cdot D_h \cdot (T_a - T_s) \quad (2)$$

$$Q_e = \rho_a L_v \cdot K_e \cdot dq/dz = \rho_a \cdot L_v \cdot D_e \cdot (0{\cdot}662/p) \cdot (e_a - e_s) \quad (3)$$

where ρ_a is the density of air, kg/m^3; C_{pa} is the specific heat of air, J/kg/°C; K_h is the eddy diffusivity for heat, m^2/s; K_e is the eddy diffusivity for water vapour, m^2/s; dT/dz is the vertical temperature gradient, °C/m; dq/dz is the specific humidity gradient, per m; L_v is the latent heat of vaporization, J/kg; p is the atmospheric pressure, mbar; e_a is the air vapour pressure at height z, mbar; e_s is the surface vapour pressure, mbar; T_a is the air temperature (°C) at height z; T_s is the surface temperature, °C; and the bulk exchange coefficient D (m/s) can be obtained as a function of wind speed and roughness lengths for neutral ($D_{(n)}$) atmospheric stability. We assumed the bulk exchange coefficient for heat, vapour and momentum were equal:

$$D_n = \kappa^2(u_z)/ln((z - h)/z_o)]^2 \quad (4)$$

where κ is von Karman's constant, 0·41; u_z is wind speed at height z, m/s; z_o is roughness length, m; and h is snow depth, m.

For non-neutral conditions, a correlation must be applied to account for the stability of the air just above the ground surface (Price and Dunne, 1976). To compensate for air stability, daily heat exchange coefficients were adjusted based on the air temperature profile between the surface and the reference height z (m), using

$D_{(s)}$ for stable, and $D_{(u)}$ for unstable conditions (Braun, 1985). This was accomplished by comparing the air temperature T_a with T_s. If T_a was less than T_s, then the stable heat transfer coefficient was used:

$$D_{(s)} = D_{(n)}/(1 + 10R_i) \tag{5}$$

where R_i is the Richardson number, defined as:

$$R_i = \frac{gz(T_a - T_s)}{u_z^2(T_a + 273{\cdot}15)} \tag{6}$$

where g is the gravitational constant, 9·81 m/s^2.

When the air density at the surface is less than the air density above the surface, an unstable situation occurs and the heat transfer coefficient is calculated thus:

$$D_{(u)} = D_{(n)}(1 - 10R_i) \tag{7}$$

When using the energy balance method for snowmelt, the average surface roughness length (z_o) in Equation (4) needs to be evaluated. A constant value for the melt period (Price and Dunne, 1976; Kane *et al.*, 1993, 1997) of 0·0013 m is assumed; the assumption of a constant value was based on the small stature of the vegetation. Hinzman *et al.* (1993b) determined this constant in Imnavait watershed from numerous wind-speed profiles between 1·5 and 10 m by:

$$z_o = \exp\left[\frac{u_2 ln(z_1) - u_1 ln(z_2)}{u_2 - u_1}\right] \tag{8}$$

where z_1 and z_2 are the two heights at which wind-speed measurements are made, m, and u_1 and u_2 are the wind speeds at the two heights z_1 and z_2 m/s.

As the snow melts, the surface roughness increases as the vegetation protrudes through the snowpack. Price and Dunne (1976) concluded, from field work in Schefferville, Quebec, Canada, that protruding small vegetation will increase the z_o from 0·005 to 0·015 m as the melt progresses. Braun (1985) used optimal values between 0·00015 m and 0·007 m; he found that these values changed from one melt period to another. Anderson (1976) used a constant value of z_o equal to 0·0005 m.

Advective heat transfer (Q_a) is the energy transferred in flowing water or rainfall. The temperatures and volumes of rainfall in the study area are typically low, so energy added to the snow through this mechanism is not very important during most of the year and particularly during snowmelt.

Similar approaches to those of Price and Dunne (1976) and Kane *et al.* (1997) were used to determine each component in Equation (1). Once the energy available for snowmelt is determined, the water equivalent of snowmelt can be determined as:

$$M = (1000Q_m)/(\rho_w \cdot L_f) \tag{9}$$

where ρ_w is density of water, kg/m^3; L_f is latent heat of fusion, J/kg; Q_m is the summation of energy available for melt per unit area for time increment of calculation; J/m^2; and M is the water equivalent of snowmelt, millimetres of water/(hour or day).

This calculation can be started at any time. No melting of the snowpack is allowed until the net energy overcomes the cold content of the snowpack. The energy input into the snowpack will be used to warm the snow until the cold content becomes zero when the snowpack is isothermal at 0°C. After that, additional energy will be used to melt snow. If the energy obtained by adding Q_{net}, Q_h, Q_e and Q_c is negative during

calculation for each time step, then the cold content increases by that amount. The initial cold content of the snowpack, when starting the calculation, can be evaluated by:

$$Q_{cc} = h \cdot \rho_s \cdot C_p \cdot (T_o - T) \tag{10}$$

where h, ρ_s and C_p are depth, m, density (kg/m^3) and heat capacity of snow, J/kg °C respectively; T is the average snow temperature, °C; T_o is the temperature of snow when it reaches isothermal condition of melting, usually 0°C. Because meltwater can readily infiltrate into the active layer and freeze, we also estimate the initial cold content of this layer and add it to the snowpack.

Adjustments are made to solar radiation to account for slope and aspect (Hinzman *et al*., 1993b).

Degree-day method. Four many areas in the Arctic we do not have the required data to calculate amounts of snowmelt based upon an energy balance. So, a simple degree-day method (Hinzman and Kane, 1991; Kane *et al*., 1993, 1997), which requires less data, has been incorporated as a secondary option. The model can be written as:

$$M = C_o(T_a - T_o)/S \tag{11}$$

when $T_a > T_o$ and where C_o is degree-day melt factor, mm/day °C, and S is time steps per day (1 day or 24 h).

In order to apply the degree-day method, the model should be started when the snow is isothermal. The approach adopted here does not consider cooling of the snowpack. Equation (11) is valid only when $T_a > T_o$. If $T_a < T_o$, then $M = 0$. The degree-day method presented here is the simplest method for determining snowmelt.

Evapotranspiration. A recent study showed that annual ET is equivalent to 30% to 60% of annual precipitation in Imnavait watershed, Alaska (Kane *et al*., 1990). In the summer with nearly 24 h of sunshine daily, the Arctic receives large amounts of radiation, relative to other seasons, of which 40% to 65% is consumed by the ET process (Kane *et al*., 1990). Mendez *et al*. (1998) reported that 45% of the net radiation was consumed for evapotranspiration in wetlands near Prudhoe Bay, Alaska. In the model herein, ET is estimated primarily by the energy balance method. The Priestley–Taylor method (Priestley and Taylor, 1972) is an optional approach to evaluating ET when data is lacking for the energy balance method. An accounting procedure maintains a water balance on each element at the end of every time step. Evapotranspiration cannot occur in the model if the moisture content extraction pressure (soil water tension) increases above the 15 bar wilting capacity (Hillel, 1980; Hinzman *et al*., 1991b) based upon the surface soil characteristic curve, which is necessary input data.

Energy balance method. The energy balance technique is a widely used method for determining evaporation and/or transpiration (Kane *et al*., 1990). It can be expressed as:

$$Q_{et} = Q_{net} + Q_h + Q_c \tag{12}$$

where Q_{et} is the energy utilized for evapotranspiration of water moisture from the surface, W/m^2; Q_{net} and Q_h can be obtained in the same way as in the process of snowmelt described previously (Kane *et al*., 1993, 1997); Q_c is conductive energy (W/m^2) between surface and subsurface and can be obtained from Fourier's Law:

$$Q_c = K_s \cdot \frac{T_x - T_s}{x} \tag{13}$$

where K_s is the thermal conductivity of soil (W/m °C) as a function of soil temperature, T_s is soil temperature (°C) at depth x below the surface (m), and T_s is soil surface temperature (°C).

The amount of water that is lost through evapotranspiration then can be evaluated as:

$$M_{et} = \frac{1000 \cdot Q_{et}}{\rho_w \cdot L_v} \tag{14}$$

where M_{et} is the water loss (mm/h or day); ρ_w is density of water, kg/m^3; and Q_{et} is summation of energy available for evapotranspiration per unit area for the time increment of the calculation, J/m^2.

Priestley–Taylor method. The Priestley–Taylor equation (Priestley and Taylor, 1972) is:

$$Q_{et} = \alpha \cdot \left(\frac{s}{s+\gamma}\right)(Q_{net} - Q_c) \tag{15}$$

where α is a parameter relating actual to equilibrium evaporation; s is the slope of the specific humidity and temperature curve at the surface, 1/°C; and γ is a psychometric constant in terms of specific humidity, 1/°C. After conducting studies at a well-drained, upland lichen heath area in a subarctic region, Rouse and Stewart (1972) and Stewart and Rouse (1976) found that α has an average value of 0·95 and that $s/(s+\gamma)$ could be simplified to a linear function of the screen air temperature as:

$$\frac{s}{s+\gamma} = 0{\cdot}406 + 0{\cdot}011\, T_a \tag{16}$$

Rouse *et al.* (1977) found that the parameter α varies with vegetation type and soil moisture content.

Flow routing. There are three different flow processes that must be included to describe the hydrology in the Arctic: subsurface flow, overland flow, and channel flow (Hinzman *et al.*, 1993a). These processes operate over similar spatial scales but markedly different temporal scales. Subsurface water flows through soil pores and therefore at low velocities in the laminar regime. Overland flow occurs when saturation of the active layer forces flow through tussocks or over very porous living plants or mosses. Both overland flow and channel flow occur in the turbulent flow regime. To maximize model efficiency, different time increments are used in the flow routing within channels ($\Delta\tau$), over the soil surface (Δt) and through the subsurface (ΔT). The size of each time step is based upon the element size, slope and hydraulic properties. The critical consideration in determining time-step size is that a parcel of water must not completely cross one element or channel segment in less than one time step. For all three flow types, the maximum time-step increment is limited by the Courant condition. To satisfy this condition, the time step is $\leqslant \Delta x/c$ (Bedient and Huber, 1992; Ciriani *et al.*, 1977), where $c = v \pm \sqrt{gy}$, Δx is the smallest grid scale of an element or channel, m; v is flow velocity, m/s; and y is the uniform water depth, m.

Subsurface flow. In the Arctic, subsurface hydrological processes are limited to the shallow active layer because continuous ice-rich permafrost is essentially an impermeable boundary to water flow. We have defined three layers within the soil profile shown as Figure 3. Any combination of soils with documented soil properties can be used. In our case the top layer is a mixture of organic soil and live vegetation and the bottom layer is mineral soil (silty glacial till) with a highly decomposed organic layer in between. The layered system of soil horizons regulates moisture movement into and through the active layer. Each layer has its own characteristics such as thickness, hydraulic conductivity and moisture-holding capacity. On the North Slope of Alaska where the model was initially developed, the near-surface organic soils are quite porous and can absorb moisture quickly in response to spring snowmelt and summer precipitation; likewise, they drain quickly. The deeper mineral layer is generally saturated throughout the summer, with the water table near the top of the mineral soil. It has a lower hydraulic conductivity. In our surface organic soils, infiltration is a very rapid process as compared with lateral flow. Infiltrating water typically only has to travel about 20 to 30 cm

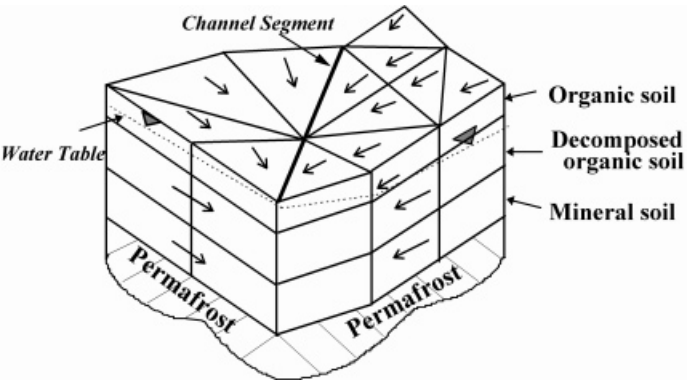

Figure 3. Schematic of the subsurface system as represented in the model

or less vertically through porous organic soils to reach the water table in the active layer. For each layer i at any element j, the flow rate is calculated by Darcy's Law:

$$q = K_i \cdot s_j \cdot A_i \tag{17}$$

where K_i is hydraulic conductivity of layer i, m/s; s_j is the slope of element j, which initially is the geographical slope, and later on is modified by considering the water table around this element, and then it becomes the slope of the hydraulic gradient; A_i is the cross-sectional area of flow for each layer, m^2, which varies depending on how flow from an element is partitioned to neighbouring elements (Figure 1e). The total amount of subsurface flow within a time step ΔT from an element j is:

$$Q_j = \sum_i K_i \cdot s_j \cdot A_i \cdot \Delta T \tag{18}$$

After each time-step calculation, the volume of water held in storage in each element is compared with its level of saturation to determine if there is subsurface flow downslope. Gravity drainage is not permitted if the moisture content extraction pressure is greater than the one-third bar field capacity (Hillel, 1980; Hinzman *et al*., 1991b). The time step ΔT for subsurface flow should be such that water will not flow past the whole element within one time increment.

Overland flow routing. The surface soils in the study area are porous organic soils where infiltration rates are high. In soils with lower infiltration capacity, overland flow tends to occur when the rate of precipitation or snowmelt exceeds the infiltration rate. However, these soils tend to become saturated from the bottom of the active layer up to the surface, and overland flow occurs when the water table rises above the surface (Hinzman *et al*., 1993a). In our model, we use the flow mechanism that overland flow (which is treated as sheet flow) exists when the water content in each element exceeds the storage capacity. The water content in each element may change with each time step, and the total storage capacity of each element may also increase or decrease as the active layer thaws or freezes.

The kinematic wave solution has been shown to be an excellent tool for most cases of overland flow calculation (Eagleson, 1970; Ciriani *et al*., 1977; Anderson and Burt, 1990). Under the kinematic wave assumption, the friction slope (S_f) and the bed slope (S_o) are equal, and Manning's equation can be used to express the relationship between flow rate and depth:

$$q = v \cdot A = \frac{C}{N} A R^{2/3} \sqrt{S_f} \tag{19}$$

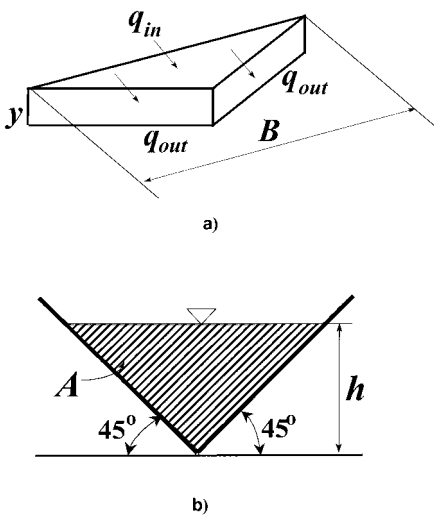

Figure 4. (a) Overland flow components within an element. (b) Channel flow cross-section

where q is the rate of lateral flow per unit length, $m^3/s/m$; v is fluid velocity, m/s; $R = A/P$ is the hydraulic radius; m; P is the wetted perimeter, m; N is the roughness coefficient for overland flow, and C is a unit factor. For a sheet flow, as assumed in this model, $R \approx y$. So Equation (19) now becomes:

$$q = \frac{C}{N} B \sqrt{S_o} y^{5/3} \tag{20}$$

The cross-sectional area is $A = B \cdot y$, as shown in Figure 4a, where the width B is the projected length on the plane perpendicular to flow direction. The overland flow balance for each element within time step Δt can be written explicitly as:

$$(\Sigma q_{\text{in}} - \Sigma q_{\text{out}}) \cdot \Delta t = \Delta s \tag{21}$$

where Δs is the change of storage in each element within Δt.

After each time step, a new total water content for each element is obtained and then the uniform water depth over each element, y, is determined by subtracting the storage capacity of the soil from the total water content. This new y is used to calculate flow rate leaving/entering each element based on Equation (20). It should be noted that when conducting mass balance for each element using Equation (21), precipitation input, evapotranspiration and contribution from subsurface flow was included. The contribution of subsurface flow to Equation (17) has been equally partitioned over ΔT. This is because the simulations of subsurface flow are calculated on a larger time increment than overland flow.

Channel flow routing. The same method as overland flow has been applied to channel flow routing. Within each reach of every channel, Manning's formula shown in Equation (19) can be applied. A triangular cross-section has been assumed for channel flow as shown in Figure 4b. So, the hydraulic radius, R, may be calculated directly from depth, h:

$$R = A/P = h^2/(2\sqrt{2}h) = h/(2\sqrt{2}) \tag{22}$$

and the mass balance and flow calculations for each channel can be characterized as:

$$(\Sigma q_{\text{in}} - \Sigma q_{\text{out}}) \cdot \Delta\tau = \Delta s \tag{23}$$

$$q = \frac{C}{2n}\sqrt{S_f} \cdot h^{8/3} \tag{24}$$

The roughness parameter for the stream channel is denoted by n. After each time step $\Delta\tau$, the mass balance is conducted based on Equation (23) by considering the amount of flow entering each channel reach from the upstream reach, the overland flow and subsurface flow from the adjacent elements, and the flow exiting each channel reach. This model does not consider loss from the stream channel back to groundwater or to evaporation. A new water depth h is then used to determine how much flow is going out during the next time step, based on Equation (24). The choice of time step $\Delta\tau$ follows the same condition as described above. Again, because channel flow ($\Delta\tau$) is simulated on a much smaller time increment than overland flow (Δt) or subsurface flow (ΔT), the contributions from overland and subsurface flows to the channel segment are equally partitioned for each Δt and $\Delta\tau$ occurring within ΔT.

Discussion of model formulation

Most distributed hydrological models have been developed for temperate regions, where the hydrological regime is dissimilar to the Arctic. In arctic regions, certain unique features associated with permafrost (such as active layer dynamics, lack of a deep groundwater component, or development of water tracks) must be adequately considered to ensure that a spatial model produces valid results. Because permafrost constrains subsurface flow within the relatively shallow active layer, subsurface flow calculations are somewhat easier compared with temperate regions where movement of groundwater is much more complicated. The active layer thaws throughout the summer, yielding a constantly varying lower boundary position, thermal and hydraulic properties, and moisture storage capacity. The presence of these characteristics that are specific to the Arctic is just one of the reasons for the development of this model.

Hinzman and Kane (1991, 1992) simulated hydrological processes using the reservoir-based HBV model (Bergström, 1976) for Imnavait Creek and have demonstrated that such a model can be used for arctic watersheds. The degree-day approach for snowmelt adequately predicted ablation and simulated flows that compared favourably with measured discharges. However, we are now faced with the problem of predicting spatially distributed soil moisture levels for use in trace gas flux models of methane and carbon dioxide from the decomposition of the abundant carbon-rich soils of the Arctic. Deriving spatially distributed soil moisture at a relatively large watershed scale was another stimulus for developing this process-based model.

Several watershed attributes in the Arctic are conducive to the development and success of a spatially distributed hydrological model. We have already mentioned the existence of permafrost and how it limits the depth of the subsurface system to be simulated. Both the lack of trees and the low diversity of arctic plants restrict the variability of the hydrological response of vegetation. Most of the areas are undeveloped, therefore the number of land surface classifications are reduced. On the negative side, the lack of hydrological and meteorological data in the Arctic limits the broad application of such models.

Although we attempted to develop a physically based model, the lack of certain data sets in even this intensely studied area resulted in some empiricism in the model. The digital terrain component of the model described here will work in any environment. The amount of topographic detail captured in the drainage network will depend upon the quality of the digital input data. We were hoping to delineate the small, hillslope water tracks in our experimental watersheds. The hydrological component of the model is presently limited to areas of continuous permafrost where any soil type(s) can be present at the surface. In our case, surface organic soils dominate not only our two study watersheds, but basically all of Alaska north of the Brooks Range. The model is executed from just prior to snowmelt through freeze-up (the time period in the autumn when snow accumulates on the surface and the soils begin to freeze). Consequently, there is no snow accumulation and redistribution algorithm. Instead we utilize spatially distributed information on the

snowpack created from field measurements made just prior to ablation. We assume that infiltration is instantaneous in the surficial organic soils, this assumption would also hold for coarse-grained soils. There are some permafrost areas where fine grained soils are present at the surface, in this case the assumption of instantaneous infiltration is not justified. For our streams, we used simple geometry for cross-sections; for small streams this is not a bad approximation. With higher order streams, actual channel cross-sections would be more realistic. We emphasize that this model is generic and that it would perform satisfactorily in most watersheds with continuous permafrost.

There are 16 parameters and 35 state variables used in the model, mostly by the energy processes. Parameter values were selected from published literature. The basin area can range from a few square kilometres to several thousand square kilometres. The time steps are dependent on the element size and topography and that the Courant condition is satisfied. Although output data are generated hourly, calculations for overland and channel flow for small elements (<50 m) may be on the time scale of minutes or seconds to satisfy the Courant condition. Data inputs such as precipitation, radiative fluxes, wind speed, relative humidity, air temperature, etc., need to be arranged as time series for each element in the basin. Basically, we took point data and kriged it over our nested watersheds to obtain these spatial and temporal data sets.

MODEL APPLICATIONS

The primary purpose for developing this model was to have the capability to examine spatial and temporal variability of moisture contents of soils in the active layer at the watershed scale. Obviously this model would prove fruitful for studying other hydrological processes. In the following sections, results from the application of this model to Imnavait Creek catchment (2·2 km^2) and Upper Kuparuk watershed (146 km^2) are presented.

Study area

The hydrological model described above was applied to two north-draining watersheds in the Kuparuk River basin on the North Slope of Alaska (Figure 5). The smaller watershed, Imnavait Creek, has been studied intensively since 1985 and the larger one, Upper Kuparuk River has been studied since 1993.

Imnavait watershed. The Imnavait watershed is a small (2·2 km^2) headwater basin located between the Toolik and Kuparuk Rivers in the northern foothills of the Brooks Range (latitude 68°30′, longitude 149°15′). This north draining basin is 78% west-facing slope, 17% east-facing slope and 5% valley riparian area. At the headwater, the hillslopes are around 10% on the west-facing slope and only slightly greater than 1% on the east-facing slope. This is in contrast to the greater than 13% west-facing slope and greater than 7% east-facing slope at the outlet. The average elevation is about 900 m (Figure 5). Most of the field measurements were conducted either in the centre of the basin on the west-facing slope where the slope averaged 10%, or on the ridge just east of the gauging site. Continuous permafrost (>250 m thickness) exists with an active layer depth of usually 40 to 60 cm. The soil profile typically has about 10 cm of surface organic soil and over 10 cm of highly decomposed organic soil. This overlies a mineral soil of glacial till. There is a thicker organic layer in the valley bottom (*c.* 50 cm) than on the ridges (*c.* 10 cm). Tussock tundra is the dominant vegetation type. Numerous water tracks are distributed over the hillslopes (Hastings *et al.*, 1989; McNamara, 1997) that are very efficient at conveying water off the slopes. Although quite obvious in aerial photographs, most of these water tracks are difficult to detect on the ground, except when flowing during snowmelt and major storms because they are not incised. Climatic data are collected at a major meteorological station in the basin. These data include precipitation, wind direction, long-wave and short-wave radiation fluxes, and profiles of wind speed, relative humidity and air temperature between the surface and 10 m elevation. Streamflow is measured in a H-flume at the basin outlet. Imnavait Creek flows parallel to the Kuparuk River for 12 km before it joins the Kuparuk River.

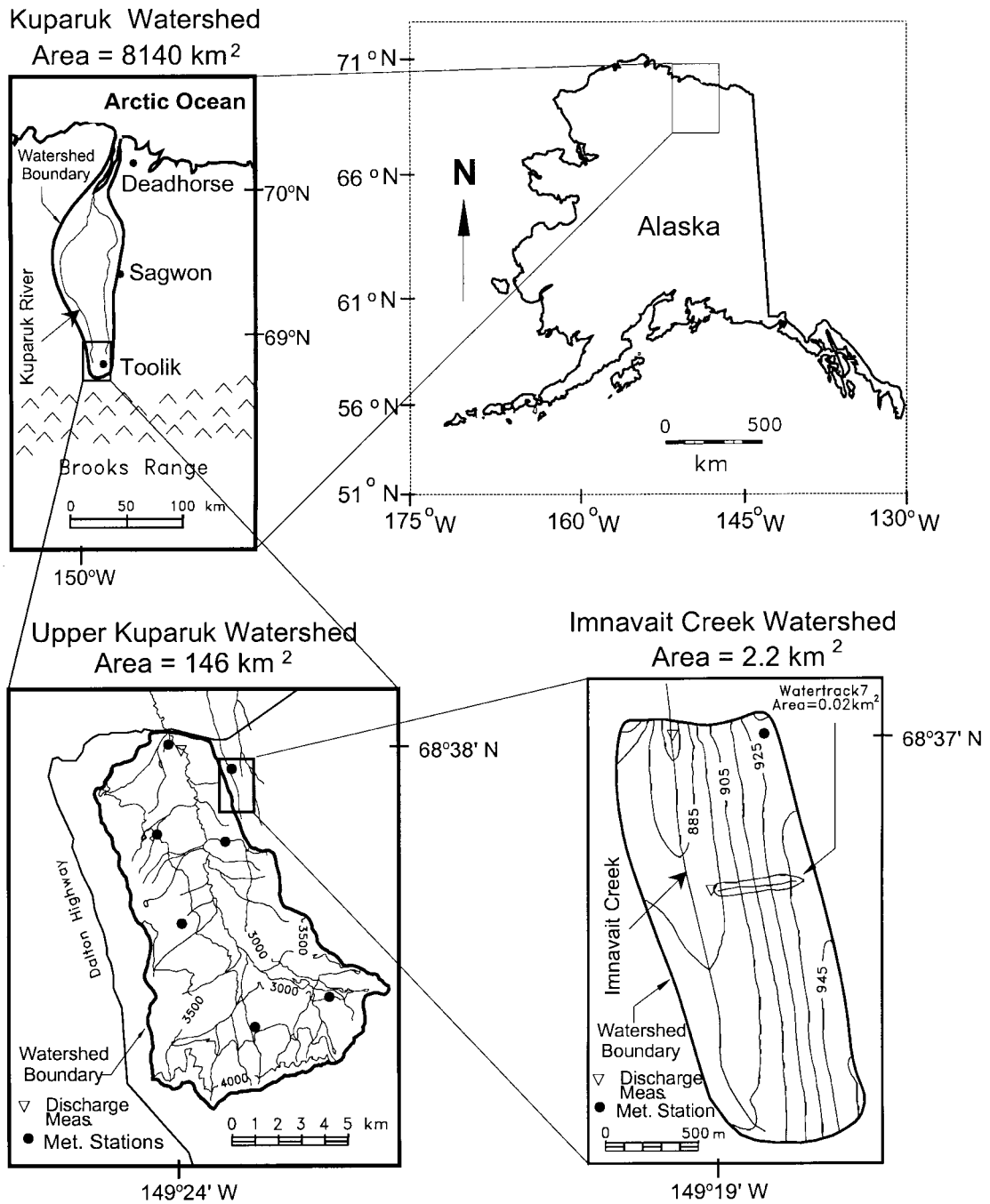

Figure 5. Nested watersheds located on the North Slope of Alaska and the meteorological stations within the Upper Kuparuk River basin

Upper Kuparuk River basin. The upper Kuparuk River basin drains 146 km^2 in the northern foothills of the Brooks Range and has many of the same attributes as Imnavait watershed. The entire Kuparuk River basin drains about 8140 km^2 at the US Geological Survey gauging site just upstream from the confluence with the Arctic Ocean. Seven meteorological stations are in or adjacent to the Upper Kuparuk River basin (Figure 5); two are major stations and five are minor stations, where only precipitation, air temperature and wind speed are measured. One major station is in Imnavait catchment and the other is near the stream gauging site on the Upper Kuparuk River. The main channel, which occupies a north-north-west trending valley, is formed at the base of steep hills. Patches of dwarf willows and birches up to 1 m in height occupy portions of the banks and water tracks. Vegetation in the basin varies from alpine at the higher elevations to moist tussock tundra at the lower elevations (Walker *et al.*, 1989).

Results of geometric analysis for arctic settings

Channel network and analysis. How an arctic watershed responds temporally and spatially to rain and snowmelt events depends upon the drainage network (McNamara, 1997). An accurate simulation of hydrological processes of a watershed depends on how well the topography is represented, channel network is delineated and flow directions within each element are determined. Stream channels and water tracks (if they exist) on the hillslopes convey water much faster than both overland flow and subsurface flow (Kane and Hinzman, 1993). If these hillslope drainage features exist and are not represented in the drainage network, hydrological simulations are not realistic.

For the Imnavait watershed, digital elevation data at a resolution of 50-m was used to delineate the channel network, whereas 300-m resolution was used in the simulations for Upper Kuparuk River basin. Plates 1a and 1b show simulated channel networks over the Imnavait watershed and Upper Kuparuk River basin. The simulated channel networks are compatible with actual channels and topography of the watershed. Most of the major water tracks are captured, particularly at the 50-m resolution. Based on the simulated channels, this model also has the ability to analyse other quantitative characteristics related to watershed delineation, such as relative stream order (Plates 1a and 1b).

Drainage area. For convenience, when digital elevation data are read into the model, the data are for a rectangular area larger than the watershed itself. This makes the DEM data set easier to prepare and to process. Although the Imnavait watershed is only 2·2 km^2, the initial rectangular model spatial domain is 5·25 km^2, consisting of 4200 triangular elements. Thus, if all the physical process simulations are based on the rectangular area, efficiency would decrease because many calculations are outside the watershed boundary. In order to save computer resources and speed up the execution of the simulation, it is useful to determine and perform computations on only the elements actually within the drainage area. By first determining channel segments that have flow contributions to the gauging site, those elements or drainage areas that contribute flow from the watershed can be obtained. The simulated drainage area of Imnavait Creek watershed is 1·9 km^2 and consists of 1512 elements (Plate 1a). For the Upper Kuparuk River basin, the rectangular area has 6448 triangular elements with an area of 290 km^2. The simulated drainage area is about 145 km^2 and consists of 3218 triangular elements (Plate 1b). The drainage areas obtained from a manual delineation from the topographic maps (1:63360) are 2·2 km^2 for the Imnavait watershed and 146 km^2 for the Upper Kuparuk River basin (McNamara, 1997). In both cases, the simulated drainage areas are reasonably close (14% and 0·7%). It should be noted that the headwaters of Imnavait watershed are complex topographically, as it is quite flat at the stream's headwater. Simulated watershed shapes are very close to actual shapes.

Hydrologic results of physical processes

Snowmelt. The energy balance approach has been used to compute rates of snowmelt. When data to calculate surface energy fluxes are not available, an alternative degree-day method can be used.

Determination of the melt factor, C_o, and the threshold value of air temperature, T_o, in the degree-day method is based on the analysis by Kane *et al.* (1993, 1997). After analysing several years of data for the Imnavait watershed, the optimized values of $C_o = 2{\cdot}7$ mm/(day $\cdot$ °C) and $T_o = -0{\cdot}2$ °C. The values of the threshold temperature are usually less than 0°C because some ablation can occur through radiative melt when the air temperature is below freezing. In our model simulation, 2·7 mm (day $\cdot$ °C) and −0·2°C have been used for C_o and T_o respectively. Kane *et al.* (1997) showed that snowmelt rates from the energy balance and degree-day methods were comparable in performance as long as C_o and T_o can be established for a range of conditions.

The index map for Imnavait watershed was obtained by averaging and normalizing the snowpack distribution measured and mapped on six consecutive years (Hinzman *et al.*, 1996). The initial snow distribution for a given year was obtained by multiplying the index map distribution by the average snowpack water equivalent. Initial snow distribution for the Upper Kuparuk River was obtained by kriging numerous spatially distributed snow measurements over the basin. Standard values were used for latent heat of fusion and vaporization, water density and specific heat of air. Field measurements of net radiation, wind speed, air temperature, atmospheric pressure, precipitation and relative humidity were spatially distributed from the seven meteorological stations (plus five microstations since 1996) in the Kuparuk basin by kriging to create distributed input files. In the simulations presented here, once the model parameters were determined (based on reported values in the literature or from field measurements), we never attempted to adjust them to improve model performance.

Figure 6 shows basin-averaged snowmelt simulation results for the Imnavait watershed in 1993, using the energy balance and degree-day methods. This is compared with average field measurements across the watershed; good agreement between simulated and measured data was attained in both cases. At the end of the snowmelt period, however, there is about a 1-day discrepancy between the two simulation methods. Note that field measurements are made daily in the morning, whereas both melt algorithms are operating at hourly time steps. During the last couple of days of melt, the snowpack is quite patchy. The existence of snow patches is related to many factors, such as local vegetation height, past wind events, initial snow depth and local topographic aspect. The performance of the model component for snowmelt by energy balance has been verified by Kane *et al.* (1997), with r^2 values from 0·97 to 0·99.

The snow distribution at the end of the accumulation season is not uniform. The depths of snow before melting can range from bare on windswept ridge tops to more than 1 m in the valley bottom (Hinzman *et al.*,

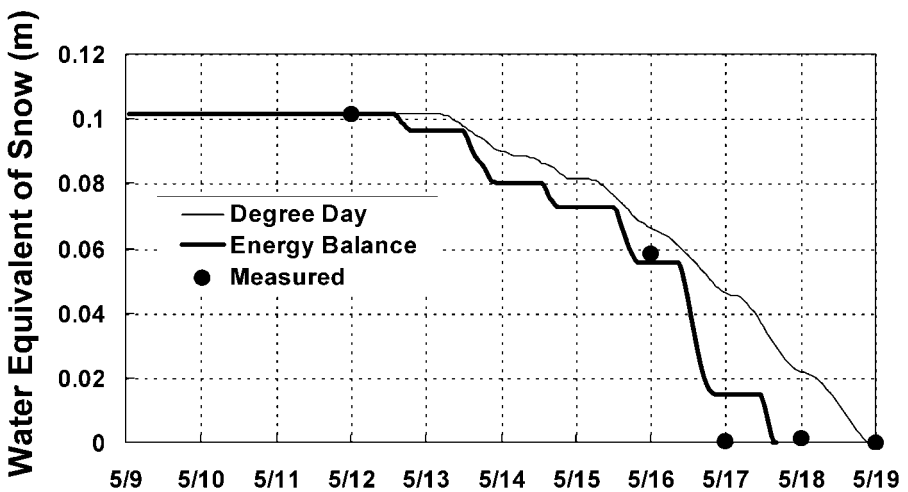

Figure 6. Comparison of snowmelt between energy balance and degree-day methods and average measured data, Imnavait watershed, Alaska, 1993

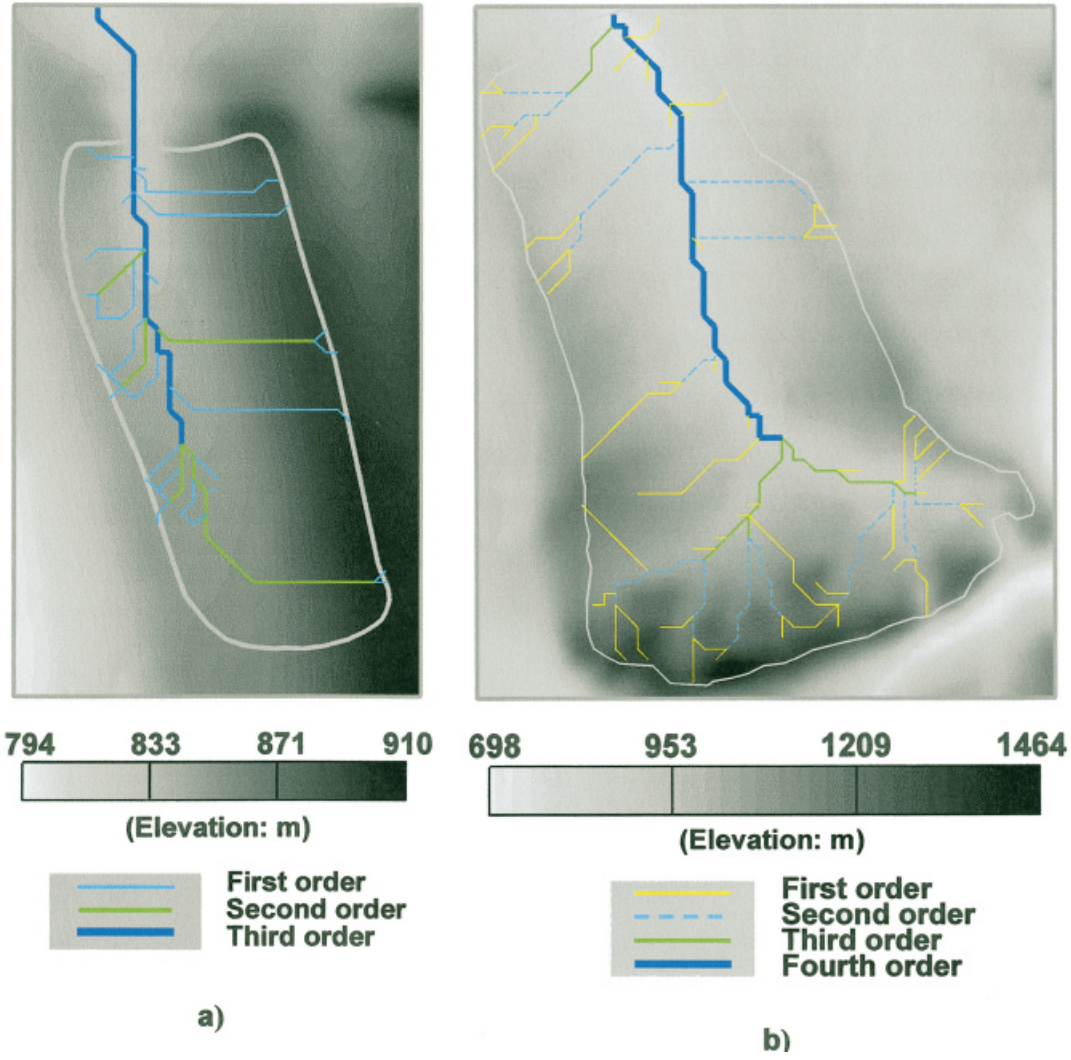

Plate 1. (a) Channel network and relative stream orders (based upon 50 m elements) of the Imnavait watershed, Alaska, (b) Channel network and relative stream orders (based upon 300 m elements) of the Upper Kuparuk River basin, Alaska.

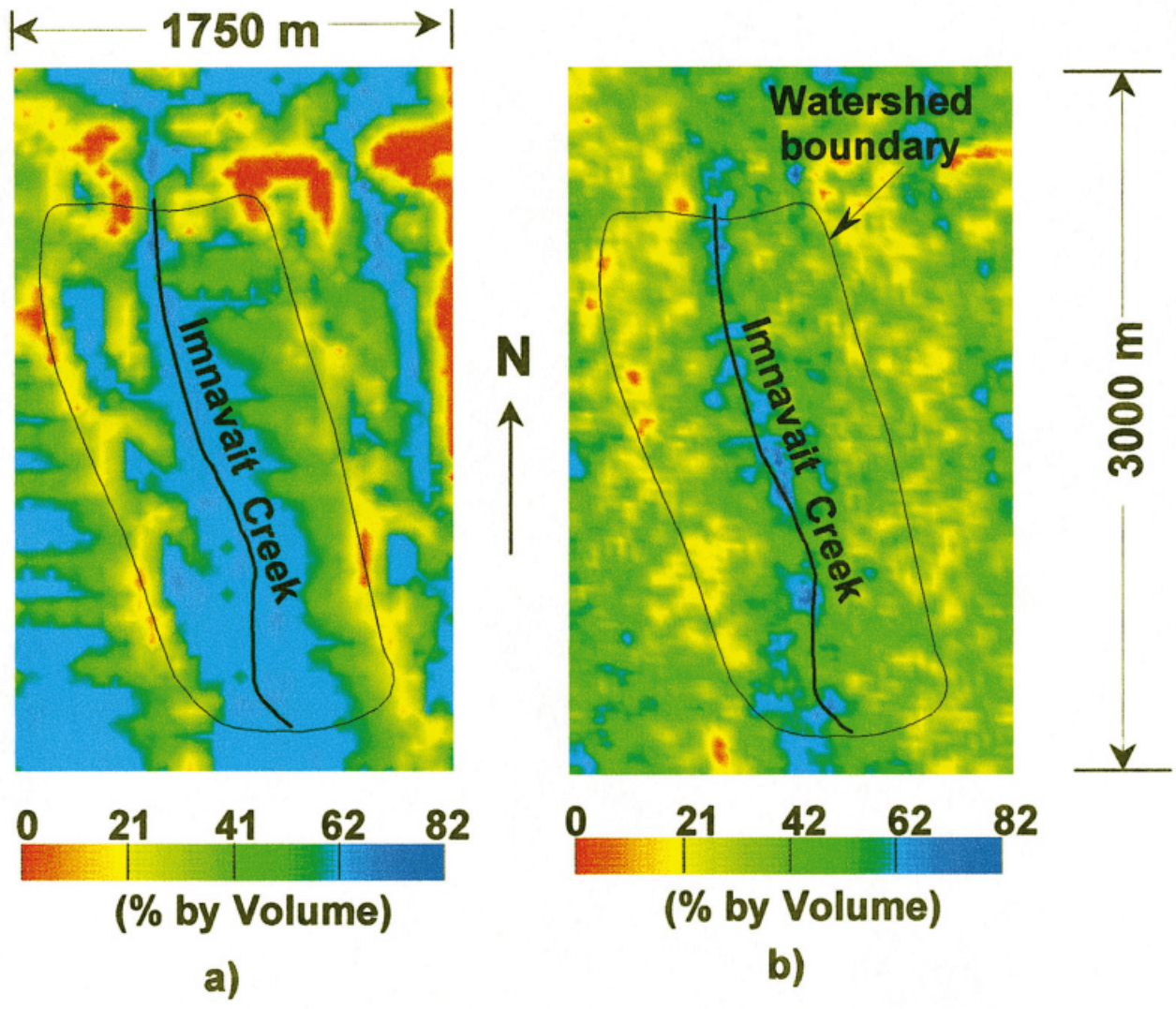

Plate 2. Simulated soil moisture content distribution (a) and SAR imagery of soil moisture content distribution (b) of Imnavait watershed at 1200 hours, 2 August 1993

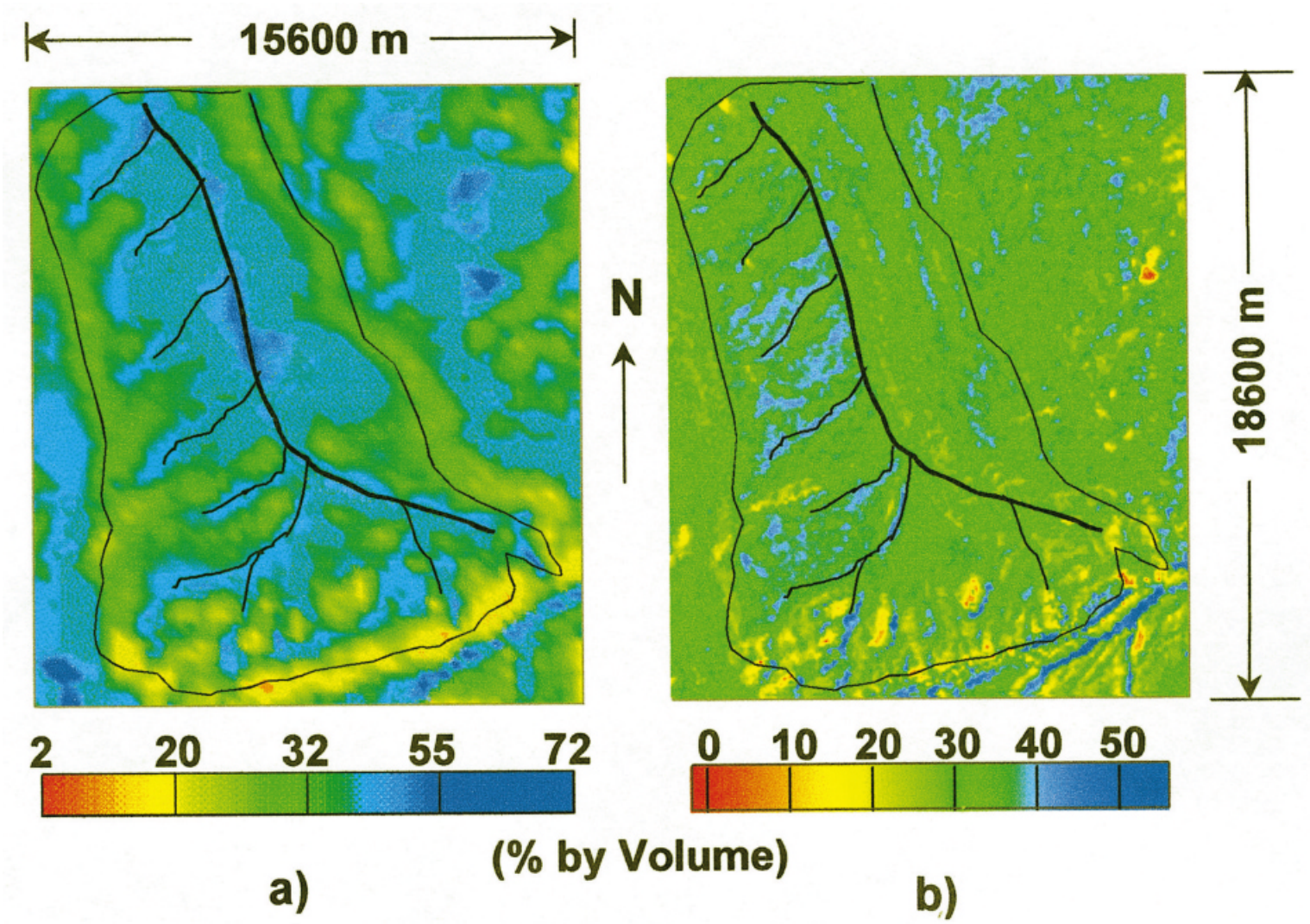

Plate 3. Simulated soil moisture content distribution (a) and SAR imagery of soil moisture content distribution (b) of Upper Kuparuk basin at 1300 hours, 15 August 1996

1996). This region has primarily north-trending katabatic winds that result from downslope drainage of denser air from the Brooks Range; however, major wind events from both the east and west are common for short periods of time. Large wind events can cause extensive drifts and wind slabs throughout the watershed, and the slab orientation depends on wind direction. The density of the drift depends partly on the magnitude of the wind events. Nevertheless, the consistency of the predominantly south-east wind yields a similar snow distribution each year, i.e., deposition in valley bottoms and on the lee side of slopes. Figures 7a and 7b show an example of spatially distributed input and output for the initial snow distribution and the distribution after four days of melting for Imnavait watershed in 1994. From Figure 7b, we can see that most of the snow in the watershed was gone (darker areas have less snow) after four days, except on the east-facing slope (whitest). The sun shines directly on the east-facing slope in the morning when the air temperature is colder and directly on the west-facing slope in the afternoon when the air temperature is warmer. This complementary input of energy causes melting to occur on the west-facing slopes faster than on the east-facing slopes. Another reason is that initially, snow was deeper on the east-facing slopes than on the west-facing slopes. This is consistent with field observations from 1985 to 1998.

The initial snow distribution used in the model for the Upper Kuparuk River basin was developed from extensive snow surveys in the basin. The rugged topography and wind events produce a very heterogeneous snowpack. Kriging was used to develop a spatially distributed map of snowpack water equivalence. Model performance was comparable to results for the Imnavait watershed. Spring snowfall events occurring after the field survey are included in the spatial distribution of precipitation data. Precipitation is treated in the model as snowfall when the air temperature is below freezing. This causes some problems in predicting accumulation from summer snowfall events because melting from the warm soils is common. Snowfall is possible on any day during the summer.

Evapotranspiration (ET). For the surface energy balance, heat conduction between surface and subsurface is considered within the upper 5 cm of organic soil profile. Hinzman *et al.* (1991b) used a guarded hot plate to determine the effective thermal conductivities of organic and mineral soils obtained from the Imnavait watershed. The conductivity was determined as a function of temperature (both when frozen and unfrozen) and moisture content. When the organic soil is thawed with moisture content near field capacity, the effective thermal conductivity is about 0·45 W/m °C. The same soil when frozen has an effective thermal conductivity of around 1·0 W/m °C. Therefore, the soil is more resistant to heat flow during the summer than during the winter, assuming similar moisture conditions.

A constant value of 0·02 m for surface roughness length in the calculation of sensible heat flux (Price and Dunne, 1976; Kane *et al.*, 1991a, 1993) was obtained by averaging several hundred wind profile measurements (Hinzman *et al.*, 1993b). There were no clear seasonal trends of surface roughness measured for the Imnavait watershed. Parameters and mass transfer coefficients used in the calculations of sensible heat flux are the same as those described in Kane *et al.* (1990).

The parameter α in the Priestley–Taylor method (Equation (14)) is modified in the following manner:

$$\alpha = \alpha_1 R + \alpha_2 \tag{25}$$

where α_1 accounts for the moisture condition of the soil and α_2 accounts for vegetation effect. A value of 1·0 for α_1 and 0·2 for α_2 is used in the model. If $R = 1$ for saturation, then $\alpha = \alpha_1 + \alpha_2 = 1{\cdot}2$. This will predict the highest combined total of surface evaporation and transpiration. Jackson *et al.* (1996) used the parameter α of 1·26 when the soil moisture deficit was zero (saturation). When R is very small, $\alpha \cong \alpha_2$ transpiration will be the only contributor to ET. Plant transpiration is also a function of soil moisture; however, this is not considered in the above equation. Evapotranspiration is calculated on the same time increment as subsurface flow (ΔT) and is one of the mass balance components.

In Imnavait watershed during the summer of 1993, the measured pan evaporation and the simulated basin-averaged evapotranspiration by the energy balance method and the optional Priestley–Taylor method are

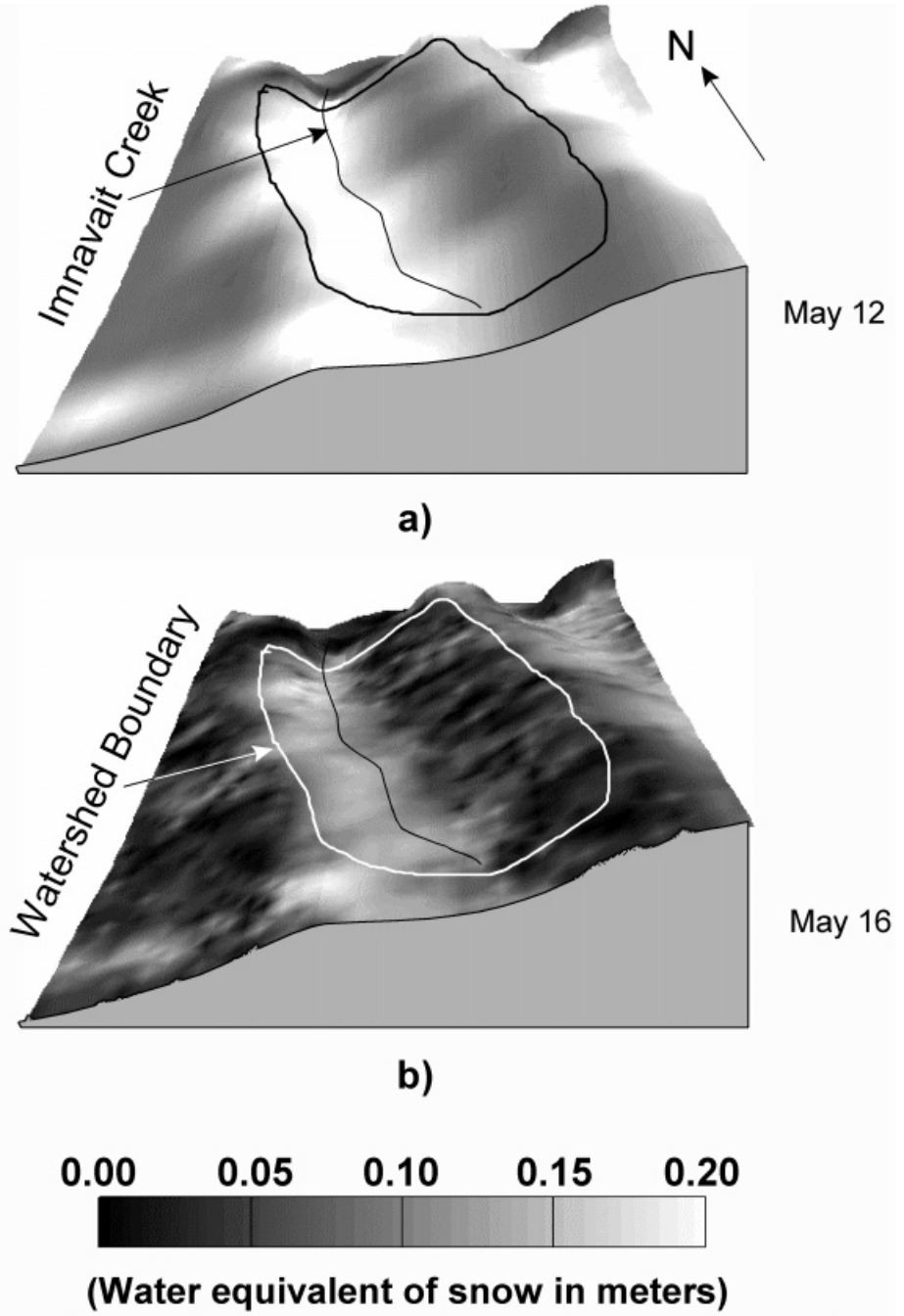

Figure 7. Initial snow distribution on 12 May 1994 (a) and simulated snow distribution after 4 days of melting (b) at Imnavait Creek watershed, Alaska

presented (Figure 8). Predicted results by both methods are similar and the summer cumulative is within 10% of that found by seasonal water balance computations. Generally, estimations from both methods are good for arctic conditions (Kane *et al*., 1990). The simulated results are less than the pan evaporation, which is an estimate of potential evaporation. Kane *et al*. (1990) studied the ET from Imnavait watershed and obtained an

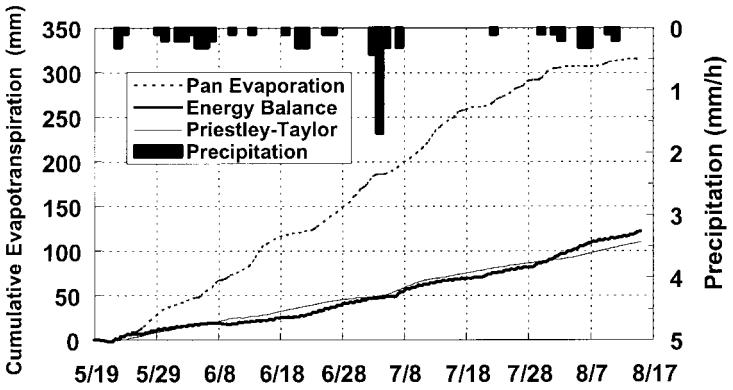

Figure 8. Comparison between measured pan evaporation and calculated basin area average evapotranspiration using the energy balance model and the Priestley–Taylor method, Imnavait watershed, Alaska, 1993

average of 0·49 (the ratio of ET over pan evaporation) during four summers based on water balance. The ratio calculated for additional unpublished data for 11 years is 0·52 and ranges from 0·34 to 0·67. The seasonal ratios of simulated ET by the energy balance and Priestley–Taylor methods over the pan evaporation for Imnavait Creek in 1993 are 0·39 and 0·35, respectively. This compares with a ratio of estimated ET from water balance computations over pan evaporation of 0·34. Although the parameters in Equation (25) were derived from published data, the validation of the equation itself needs to be tested further.

Flow routing and moisture content simulation. Subsurface flow routing. There are three different soil types within the active layer of the Imnavait watershed. Hinzman *et al.* (1991b) analysed soil samples taken from the Imnavait watershed and found that the hydraulic conductivity of the top 10 cm of organic soil averages about 15×10^{-5} m/s and the next 10 cm of highly decomposed organic soil averages about $3{\cdot}5 \times 10^{-5}$ m/s. The rest of the active layer is mineral soil, which has a conductivity of 1×10^{-5} m/s. During the summer there is basically no change in the hydraulic conductivity after the soil thaws. A 1-h time step (ΔT) was used in the calculation of subsurface flow through the soils. Based on the hydraulic conductivity of surface organic soils and the maximum slope of the watershed, the distance of subsurface water movement in 1 h is approximately 0·25 m, which is smaller than the grid scale for each element. The same time step was used for the calculation of subsurface flow in the Upper Kuparuk River basin. The active layer starts thawing after snowmelt, continues to thaw during the summer, and reaches its maximum thickness in the autumn. So the soil depth in the Darcy's equation potentially changes with each time step. Soil moisture capacities for each soil layer also change, because they are related to the soil depth. The same soil properties have been used for the Upper Kuparuk River basin as for the Imnavait watershed. In the Upper Kuparuk River basin, on some steep slopes there is no vegetation and bedrock is exposed; however, these site-specific soil features were not incorporated into the model because they represent a small percentage of the basin and have not been mapped in detail. The Reynold's number was evaluated to guarantee that the subsurface flow is laminar and that Darcy's law could be used.

Overland flow routing. Because the overland flow velocities are higher than those for subsurface flow; a smaller time step was used in the model. According to the Courant condition (Ciriani *et al.*, 1977; Bedient and Huber, 1992), for the grid scale of 50 m (Imnavait watershed) and 300 m (Upper Kuparuk River basin), if we conservatively picked a value of 0·05 m/s as the velocity and 0·02 m as the flow depth, then the estimated time step (Δt) for overland flow should be less than 101 s. A Δt of 1 min was used in actual simulations for both the Imnavait watershed and the Upper Kuparuk River basin. Roughness coefficient values (N for overland, n for channels) for overland flows in Manning's equation are typically greater than

that for channel flow. Bedient and Huber (1992) summarized some N values based on field and laboratory data. For the arctic environment, we used the roughness parameter $N = 0{\cdot}3$ in overland flow routing, which is typical for grass-covered ground.

Channel flow routing. Similar to the analysis of overland flow, the time step ($\Delta\tau$) for channel flow was adopted as 2 s, assuming that the flow velocity is less than 1·0 m/s and the depth is less than 2 m. Bedient and Huber (1992) and Chaudhry (1993) also compiled similar tables for channel flow, showing a range of values of Manning's coefficient n for different conditions. A value of 0·03 has been used in these simulations for channel flow routing. Mass balance is also conducted in each time step of $\Delta\tau$ for each channel segment, and new water depth is obtained for the next time step. The amount of water contributed by overland flow is evenly partitioned over $\Delta\tau$ for each Δt. Because hourly measured hydrograph data were available at the gauging stations on the Imnavait Creek and Upper Kuparuk River, hourly hydrograph data from the model were retained for comparison.

Discussion of model performance

Data input. One requirement for correctly utilizing a distributed model is the availability of distributed input data. In this model, hourly meteorological data were used. The required input data at 1-h step include net radiation, incoming short-wave radiation, reflected long-wave radiation, air temperature, wind speed, relative humidity, atmospheric pressure and rainfall (plus any snow in summer). Initially, distributed snow data are required. For the Imnavait watershed, data (assumed to be uniformly distributed) measured at one point within the 2·2 km^2 watershed were used. Since 1996, we utilize all of the stations in the Kuparuk basin for generating a distributed data set. The most important input variable, rainfall, as with the other variables, was treated approximately as uniformly distributed over the watershed prior to 1996. In reality, non-uniformly distributed rainfall exists during convective storms in the summer. So, some error is introduced even at this small scale.

For the Upper Kuparuk River basin, the assumption of uniformly distributed data is no longer appropriate because of the large area and mountainous terrain. Prior to 1996, we had only seven meterological sites in the whole of the Kuparuk basin, with two in/near the Upper Kuparuk River basin; five additional precipitation stations were added in the Upper Kuparuk River basin in 1996. We were able to obtain hourly, distributed data for use in the model from the seven meteorological stations located throughout the 146 km^2 basin (Figure 5). The model performance was greatly improved, compared with the simulations (not shown) conducted prior to obtaining the distributed rainfall precipitation data in 1996.

The soil layers in the active layer are initially completely frozen and are assumed to have zero liquid moisture content; the ice in the soil melts when the soil starts thawing. Most parameters related to soil hydraulic and thermal properties were adopted from other independent studies in the region. However, as there are no soil maps (only maps of vegetation), it is difficult to spatially distribute soil properties accurately. This is not as critical here as in non-permafrost watersheds, because of the limited storage involved in the active layer above the permafrost and because the area is undisturbed. Because of the data limitations, some parameters were not distributed, such as roughness for overland flow and channel flow. Also in these simulations, the depth of thaw was not predicted spatially.

Verification. The quality of output from models is closely aligned with the quality of the parameters and input data used to drive them. Spatially distributed models typically require greater amounts of input data, making this truism even more relevant. To adequately evaluate a spatially distributed model, it is necessary to have independent spatial data sets. Applying remotely sensed data is the most appropriate approach for this purpose. For example, Wigmosta *et al*. (1994) used AVHRR satellite data to monitor the distribution of snow in the watershed and compared this with simulated results during ablation. We have measured near-surface soil moistures with synthetic aperture radar (SAR) and used this to evaluate the spatial performance

of this model. This technique shows promise in this region of the world because of the limited height of vegetation and the relationship between surface and subsurface moisture contents.

Grayson *et al.* (1992) raise the issue that model development typically is not in concert with field programmes designed to test the models and therefore the linkage to reality is lost. In this study, we were fortunate to have the resources to carry out a field programme in parallel with the model development. It would have been futile to proceed with developing the model without a field programme in the Arctic; the data to test the model does not presently exist for many other catchments.

Moisture distribution. Prediction of spatially distributed moisture over a watershed is one of the most important products of this model. However, it is cost prohibitive to make sufficient field measurements to map soil moisture variation on the watershed scale. In our model, moisture distribution results can be generated for each time step (ΔT) of the whole simulation period, whereas satellite imagery by comparison is received at a minimum once every few days. Plate 2a shows the simulated moisture content distribution over Imnavait watershed on 2 August 1993. The model results are qualitatively correct because they show ridges to be the driest, the valley bottom to be the wettest, and the hillslope to be in between them. In order to verify the distributed model results, spatially derived soil moisture data from SAR images at the same location and time were used (Plate 2b) (Goering *et al.*, 1995; Kane *et al.*, 1996). This technique is still in the development; however, reasonable results have been obtained for this treeless region. Simulated soil moisture contents in Plate 2a represent average values for the upper 10 cm of the active layer, whereas the SAR results are from the top 2 cm (depth of penetration). Therefore, it was expected that as the porous organic soils drain vertically, the simulated results would be higher than the SAR results as shown in Plate 2b. The predicted and SAR soil moisture distribution for the Upper Kuparuk River basin is shown for 15 August 1996 in Plates 3a and 3b. Again, it is quite easy to locate the drier ridges, wet valley bottoms, and the intermediate wet slopes, with both figures being qualitatively similar. Although histograms of distributed soil moisture from SAR and simulations over the watershed have similar shapes, the distribution is offset, with SAR showing a drier catchment. One discrepancy is the simulated soil moisture distribution and SAR imagery of soil moisture distribution on the east side of Upper Kuparuk River. The reason is that SAR imagery was based on a 50-m DEM, and some small ridges exist on the east side of Upper Kuparuk River basin that block the water from flowing toward the main stream, shunting it northward. In the model simulation, 300 m DEM was used and small drainage features were not captured.

Discharge. The classic verification of model performance is to compare measured and predicted hydrograph data. Figures 9a and 9b show the measured and predicted hydrograph data for the Imnavait watershed in 1993 and 1994, respectively. Figure 10 shows similar results for the Upper Kuparuk River basin in 1996. There are some discrepancies between the measured and predicted results. Our model predicts that snowmelt runoff is initiated a few days before it actually occurs, because an algorithm for snow damming has not been incorporated in the model. Recall that the valley bottoms are the same areas where excessive amounts of wind-packed snow have accumulated. Calculations of snowmelt and flow routing can also contribute minor discrepancies between measured and predicted discharges. The predicted cumulative discharge volume is comparable to the measured cumulative discharge volume (Figures 9 and 10).

The model performance of discharge calculation generally relies upon three criteria: visual inspection of simulated and measured hydrographs, visual inspection of cumulative discharge between simulated and measured hydrographs, and the r^2, Nash–Sutcliffe coefficient (Martinec and Rango, 1989) which is calculated as:

$$r^2 = 1 - \frac{\sum_{t=1}^{n} [Q_{\text{sim}}(t) - Q_{\text{meas}}(t)]^2}{\sum_{t=1}^{n} [Q_{\text{meas}}(t) - \bar{Q}_{\text{meas}}]^2} \tag{26}$$

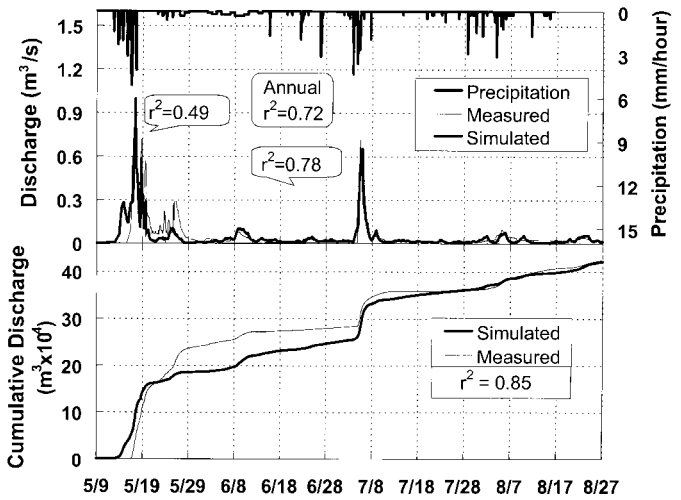

a)

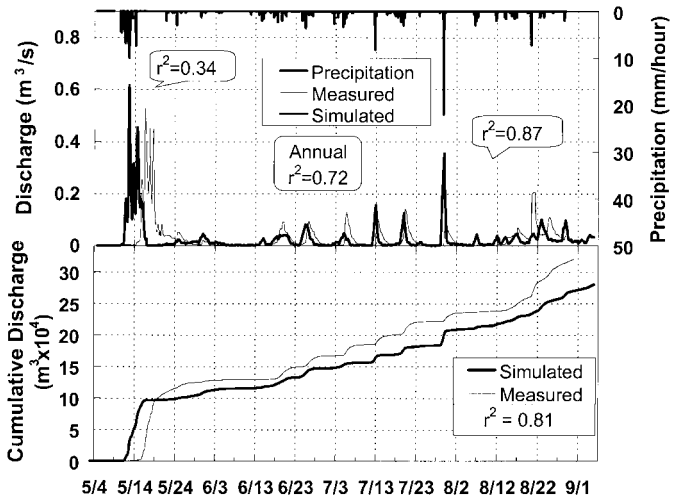

b)

Figure 9. Comparison of simulated and measured discharges and cumulative volume of simulated and measured discharges (a) at Imnavait Creek, Alaska, 1993 and (b) at Imnavait Creek, Alaska, 1994

where Q_{sim} is simulated discharge (or cumulative simulated discharge) (m^3/s), Q_{meas} is measured discharge (or cumulative measured discharge) (m^3/s), with:

$$\bar{Q}_{\text{meas}} = \frac{1}{n}\sum_{t=1}^{n} Q_{\text{meas}}(t) \quad (m^3/s) \tag{27}$$

t is the time variable (days or hours) and n is the number of time steps.

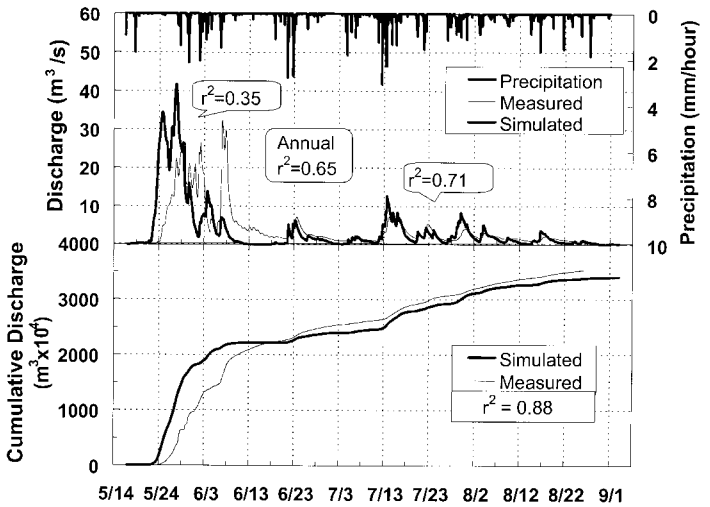

Figure 10. Comparison of simulated and measured discharges and cumulative volume of simulated and measured discharges at Upper Kuparuk, Alaska, 1996

The r^2 for the summer runoff period is 0·78 and 0·88 for Imnavait watershed in 1993 and 1994 and 0·71 for the Upper Kuparuk River basin for 1996 (Figures 9a, 9b and 10). The r^2 values are less impressive for the snowmelt period (0·49 and 0·34 for Imnavait watershed and 0·35 for the Upper Kuparuk River catchment); these values could be improved substantially if an algorithm for the snow damming process was developed for this area. In each case, the predicted runoff from snowmelt is too early and the simulated peaks are too high. The mechanism that triggers the initial slush flow release is very difficult to predict, because the catastrophic event could initiate anywhere in the valley bottom when the weight of the wet snow overcomes some threshold resistance to flow. The r^2 of the cumulative curves (Figures 9a, 9b and 10) for combined snowmelt and summer runoff are quite good, exceeding 0·8 for each.

For the Imnavait watershed in 1993 and 1994 and the Upper Kuparuk River basin in 1996, the predicted and measured (estimated from water balance) ET, snowmelt runoff, summer runoff and total runoff (Figure 11) were compared for the period from snowmelt to freeze-up. Predicted ET by the energy balance and the Priestley–Taylor methods were compared with the estimate from the water balance. The comparisons for the Imnavait watershed indicate a difference of 15%. For the Upper Kuparuk catchment, ET and snowmelt runoff are overestimated and summer runoff is underestimated. The Imnavait watershed has more uniform characteristics (soil properties, gentler topography and less variation in air temperature, wind speed, etc.) partially because of its small size and it has been studied in more detail than the Upper Kuparuk River basin. The lower r^2 values for simulated runoff in the Upper Kuparuk River basin were expected. Recall also that the element size was increased for the Upper Kuparuk basin by a factor of six; this resulted in the loss of topographic detail that cascades through all of the routing routines (subsurface, overland and channel).

Other issues. Owing to the existence of permafrost, the subsurface flow system is physically limited to the thin active layer. This makes it relatively easy to measure the moisture regime and determine hydraulic properties for the model. In most other watershed studies, modelling of subsurface processes is very difficult because of anisotropic and heterogeneous properties of soils and bedrock and the deep groundwater aquifers with large storage reservoirs (Grayson *et al*., 1992; Wigmosta *et al*., 1994; Jackson *et al*., 1996). Within the active layer, the surface organic soils are highly porous and infiltration rates are high. In our model, the travel time from the ground surface to the water table in the active layer during infiltration by water is neglected,

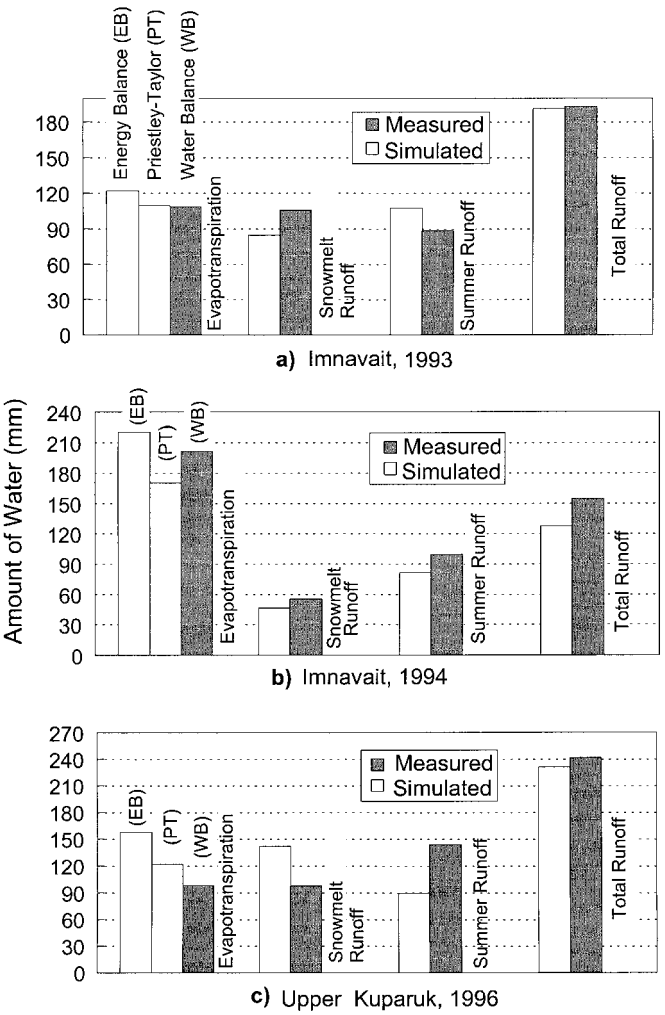

Figure 11. Comparison of cumulative hydrological components that were measured and simulated for Imnavait and Upper Kuparuk watersheds from snowmelt to freeze-up

because it is short compared with the travel time of flow down the hillslopes. We also made the same assumption for the thin snowpack; vertical travel times are only significant in deep snowdrifts.

Because vegetation in the Arctic is relatively small, many of the problems associated with precipitation and radiation distributions at various levels in the canopy are eliminated. In our energy budget algorithms for evapotranspiration and snowmelt, we use either measured net radiation or calculate the net radiation from measured long-wave and short-wave radiation at each major meteorological site.

Channel networks are created based on the DEM data. The amount of detail generated by the DEM algorithm depends upon the size of the elements used and the format of the digital elevation data. For the Imnavait watershed, the triangular elements were 50 m by 50 m and for the Upper Kuparuk River they were 300 m by 300 m. For larger elements, the likelihood of capturing water tracks is reduced. This is confirmed by the soil moisture results for the Upper Kuparuk watershed in Plates 3a and 3b. Field observations confirm that water tracks are very efficient at removing water off the hillslopes and should be incorporated in the drainage network used in the model.

In our model, a simple triangular cross-section was assumed for channel and water tracks and one value of channel roughness was used. Using other cross-sectional shapes and values for channel roughness may help improve model performance.

Model weaknesses. Three areas where modelling results could be improved are: (i) an algorithm for snow damming, (ii) use of smaller spatial elements so that more topographic details (such as water tracks) are captured, and (iii) improve our data collection network to better represent spatial variability or use regional climatic models to obtain the spatial data information. For area (i), a good predictive algorithm for the snow damming process does not exist; from field observations, snow damming retards snowmelt runoff for several days and results in higher peak flows than would occur without this process. For area (ii), as the watershed size to be modelled increases, it becomes a computational necessity to increase element size. Also, this results in the more subtle water tracks not being depicted in the simulated drainage network.

Finally for area (iii), some of the discrepancies between simulated and measured results are due to the quality of the input data. With the exception of one gauging station operated by the US Geological Survey and three Wyoming snow gauges run by the US Department of Agriculture, we collected the data used in this study. Financial constraints and the lack of certain data bases, such as soil maps, restricted the amount of input data available for model use.

CONCLUSIONS

A process-based, spatially distributed hydrological and thermal model has been developed for arctic regions; the first of this kind for areas of continuous permafrost. The model consists of two parts: watershed drainage network delineation and hydrological process simulations that include energy-related processes such as snowmelt, ground thawing and evapotranspiration. Although not all simulated process-related results could be compared with measured values, those that were showed good agreement as demonstrated by the r^2 values. We believe that we have demonstrated that process-based, spatially distributed models can perform satisfactorily under certain conditions. Because the permafrost acts as an aquitard, the subsurface system is greatly simplified and therefore easier to model. Owing to the restricted subsurface storage, the variation from year-to-year in the volume of water stored in the active layer is small.

As we scaled up from the small 2·2 km^2 Imnavait Creek to the 146 km^2 Upper Kuparuk River, element size increased by a factor of six. This resulted in some loss of topographic detail on the hillslopes whereby only the larger water tracks were captured. This loss of topographic detail cascaded down through all three of the routing algorithms (subsurface, overland and channel flows).

For models of the type presented here, it is important to have good quality input data that can be spatially distributed throughout the watershed with some level of confidence. The field data collection programme was designed specifically to support model applications presented here. Both the modelling and the field research efforts proceeded in parallel, this allowed us to modify our data collection programme and model formulation as needed. For the Upper Kuparuk River we consistently did not have sufficient precipitation distributed as input over our watershed to reproduce the amounts of runoff measured. At this point we added five additional rain gauges in the headwaters that substantially improved our runoff forecasts.

This model is capable of simulating distributed processes such as snowmelt, subsurface flow, overland flow, channel flow, soil thawing and evapotranspiration. A true test of this model would be the comparison of simulated and measured spatially distributed data. We attempted to do this, unfortunately the model outputs cannot be directly compared with SAR estimates of soil moisture. The model output is an average for the top 10 cm, whereas the SAR results are for the top 2 cm. It is encouraging that the soil moisture distribution looks reasonable when compared with the topography (ridges are dry, valley bottoms wet and hillslopes at intermediate levels). The distributions between the simulated results and SAR estimates of soil moisture are quite similar, but they are offset, with the SAR results being lower.

Phase change is an important process in the arctic hydrological cycle. We have tried to make the thermal components of our model as robust as possible. Accurately depicting snowmelt is important, as it is usually the dominant hydrological event each year. Evapotranspiration is important during the summer because it is the main export mechanism of water out of the watershed. Finally, it is important in subsurface simulations to accurately depict the depth of the active layer that continually thaws throughout the entire summer.

Some components of the model require further refinement. We have just recently incorporated a physically based, spatially distributed thawing/freezing subroutine (Hinzman *et al*., 1998). The effects of snow damming, as often seen during the snowmelt season in the headwater basins have not been incorporated in this model yet. We would also like to explore further uses of remotely sensed data, as this is the only logistical possibility of obtaining spatially distributed data. This model is presently being applied to a watershed in the Siberian Arctic (5·5 km^2) and the entire Kuparuk River basin (8140 km^2).

ACKNOWLEDGEMENTS

This work was supported by the US National Science Foundation under the Arctic System Science (ARCSS) Land Atmosphere Ice Interactions (LAII) Program (Grant Nos OPP-9214927 and OPP-981835). We thank Robert E. Gieck, Yuwu Zhang, Elizabeth K. Lilly and Shu Li and all of the graduate students that have collected data for their involvement in this project.

REFERENCES

Abbott MB, Bathurst JC, Counge JA, O'Connell PE, Rasmussen J. 1986. An introduction to the European Hydrological System — Systéme Hydrologique Européen 'SHE': 2. Structure of the physically based, distributed modeling system. *Journal of Hydrology* **87**: 61–77.

Alley RB. 1995. Resolved: the Arctic controls global climate change. Arctic oceanography: marginal ice zones and continental shelves. *Coastal and Estuarine Studies* **49**: 263–283.

Anderson EA. 1976. *A Point Energy and Mass Balance Model of a Snow Cover*, NOAA Technical Report NWS 19. US Department of Commerce, National Weather Service: Spokane, WA.

Anderson MG, Burt TP. 1990. *Process Studies in Hillslope Hydrology*. Wiley: Chichester.

Bedient PB, Huber WC. 1992. *Hydrology and Floodplain Analysis*. Addison-Wesley: Reading, MA.

Bengtsson L. 1984. *Snowmelt Induced Urban Runoff in Northern Sweden* Report Series A(8). Hydrological Division, Department of Physical Geography University of Uppsala: Uppsala.

Benson CS. 1982. *Reassessment of Winter Precipitation on Alaska's Arctic Slope and Measurements on Flux of Wind Blown Snow*. Research Report UAG R-288, Geophysics Institute, University of Alaska: Fairbanks, AK.

Bergström S. 1976. *Development and Application of a Conceptual Runoff Model for Scandinavian Catchments*, Report RH07. Swedish Meteorological and Hydrological Institute: Norrköping.

Bergström S. 1986. Recent development in snowmelt–runoff simulation. In *Proceedings: Cold Region Hydrology*, Kane DL (ed.); Fairbanks, Alaska; 461–468.

Beven KJ. 1996. A discussion of distributed hydrological modeling. In *Distributed Hydrological Modelling*, Abbott MB, Refsgaard JC (eds); 22. Water Science and Technology Library: 255–278.

Beven KJ, Kirkby MJ. 1979. A physically-based, variable contributing area model of basin hydrology. *Hydrological Sciences Bulletin* **24**(1): 43–69.

Beven KJ, Wood EF. 1983. Catchment geomorphology and the dynamics of runoff contributing areas. *Journal of Hydrology* **65**: 139–158.

Braun LN. 1985. *Simulation of Snowmelt–Runoff in Lowland and Lower Alpine Regions of Switzerland*, Zücher Geographische Schriften, Geographische Institut Eidgenössische Technische Hochschule: Zürich; Heft 21, 166 pp.

Chaudhry MH. 1993. *Open-Channel Flow*. Prentice-Hall: Englewood Cliffs, NJ.

Ciriani TA, Maione U, Wallis JR. (eds) 1977. *Mathematical Methods for Surface Water Hydrology*. Wiley: Chichester.

Clagett GP. 1988. The Wyoming windshield — an evaluation after 12 years of use in Alaska. In *Proceedings, Western Snow Conference* (Vol. 56). Western Snow Conference: Beaverton, Oregon; 113–123.

Crawford RMM (ed.). 1997. *Disturbance and Recovery in Arctic Lands: an Ecological Perspective*. NATO Advanced Science Institutes Series: (NATO ASI) Partnership Sub-Series: 2 Environment Volume No. 25, Kluwer Academic Publishers: Dordrecht.

Eagleson PS. 1970. *Dynamic Hydrology*. McGraw-Hill: New York.

Gary NK, Sen DJ. 1994. Determination of watershed features for surface runoff models. *Journal of Hydraulic Engineering, ASCE* **120**(4): 427–447.

Goering DJ, Chen H, Hinzman LD, Kane DL. 1995. Removal of terrain effects from SAR satellite imagery of arctic tundra. *IEEE Transactions on Geoscience and Remote Sensing* **33**(1): 185–194.

Goodrich DC. 1990. Geometric simplification of a distributed rainfall–runoff model over a range of basin scales. PhD dissertation, Department of Hydrology and Water Resources, University of Arizona, Tucson.
Grayson R, Moore ID, McMahon TA. 1992. Physically based hydrologic modeling: 1. A terrain-based model for investigative purposes. *Water Resources Research* **28**(10): 2639–2666.
Hastings SJ, Luchessa SA, Oechel WC, Tenhunen JD. 1989. Standing biomass and production in water drainages of the foothills of the Philip Smith Mountains, Alaska. *Holarctic Ecology* **12**: 304–311.
Hillel D. 1980. *Fundamentals of Soil Physics*. Academic Press: New York.
Hinzman LD, Kane LD. 1991. Snow hydrology of a headwater arctic basin: 2. Conceptual analysis and computer modeling. *Water Resources Research* **27**(6): 1111–1121.
Hinzman LD, Kane LD. 1992. Potential response of an arctic watershed during a period of global warming. *Journal of Geophysical Research* **97**(D3): 2811–2820.
Hinzman LD, Kane DL, Gieck RE. 1991a. Regional snow ablation in the Alaskan Arctic. In *Northern Hydrology, Selected Perspectives*, Prowse TD, Ommanney CSL (eds); NHRI Symposium No. 6, National Hydrology Research Institute: Saskatoon, Saskatchewan; 121–140.
Hinzman LD, Kane DL, Gieck RE, Everett KR. 1991b. Hydrologic and thermal properties of the active layer in the Alaskan arctic. *Cold Regions Science and Technology* **19**: 95–110.
Hinzman LD, Kane DL, Everett KR. 1993a. Hillslope hydrology in an Arctic setting. *Sixth International Conference on Permafrost*, 5–9 July, Beijing; 267–271.
Hinzman LD, Wendler G, Gieck RE, Kane DL. 1993b. Snowmelt at a small Alaskan arctic watershed: 1. Energy related processes. In *Proceedings of the 9th International Northern Research Basins Symposium/Workshop, Canada, 1992*, Prowse TD, Ommanney CSL, Ulmer K (eds); (Vol. 1), NHRI Symposium, No. 10. National Hydrology Research Institute: Saskatoon, Saskatchewan; 171–226.
Hinzman LD, Kane DL, Benson CS, Everett KR. 1996. Energy balance and hydrological processes in an Arctic watershed. In *Landscape Function and Disturbance in Arctic Tundra*, Reynolds JF, Tenhunen JD (eds); (Vol. 120), Ecological Studies. Springer-Verlag: Berlin; 131–154.
Hinzman LD, Goering DJ, Kane DL. 1998. A distributed thermal model for calculating temperature profiles and depth of thaw in permafrost regions. *Journal of Geophysical Research — Atmospheres* **103**(D22): 28975–28991.
Jackson TH, Tarboton DG, Cooley KR. 1996. *A Spatially-distributed Hydrologic Model for a Small Arid Mountain Watershed.* Working Paper WP-96-HWR-DGT/002, Utah Water Research Laboratory: Logan, UT.
James WP, Kim KW. 1990. A distributed dynamic watershed model. *Water Resources Bulletin* **26**(4): 587–596.
Jonch-Clausen T. 1979. *SHE, Systéme Hydrologique Européen, a Short Description*. Danish Hydraulic Institute: Hørsholm, Denmark.
Jones NL, Wright SG, Maidment DR. 1990. Watershed delineation with triangle-based terrain models. *Journal of Hydraulic Engineering, ASCE* **116**(10): 1232–1251.
Kane DL, Hinzman LD. 1993. Use of spatially distributed data to model arctic hydrologic processes. In *Proceedings of Sixth International Conference on Permafrost*. Beijing; 326–331.
Kane DL, Hinzman LD, Benson CS, Everett KR. 1989. Hydrology of Imnavait Creek, an arctic watershed. *Hydrologic Ecology* **12**: 262–269.
Kane DL, Gieck RE, Hinzman LD. 1990. Evapotranspiration from a small Alaskan arctic watershed. *Nordic Hydrology* **21**: 253–272.
Kane DL, Hinzman LD, Benson CS, Liston GE. 1991a. Snow hydrology of a headwater arctic basin: 1. Physical measurements and process studies. *Water Resources Research* **27**(6): 1099–1109.
Kane DL, Hinzman LD, Zarling JP. 1991b. Thermal response of the active layer to climatic warming in a permafrost environment. *Cold Regions Science and Technology* **19**: 111–122.
Kane DL, Gieck RE, Wendler G, Hinzman LD. 1993. Snowmelt at a small Alaskan arctic watershed: 2 Energy related modeling results. In *Proceedings of the 9th International Northern Research Basins Symposium/Workshop, Canada, 1992*, Prowse TD, Ommanney CSL, Ulmer K (Eds); (Vol. 1), NIHRI Symposium, No. 10. National Hydrology Research Institute: Saskatoon, Saskatchewan; 227–247.
Kane DL, Hinzman LD, Yu H, Goering DJ. 1996. The use of SAR satellite imagery to measure arctic layer moisture contents in arctic Alaska. *Nordic Hydrology* **27**: 25–38.
Kane DL, Gieck RE, Hinzman LD. 1997. Snowmelt modeling at a small Alaskan arctic watershed. *Journal of Hydrologic Engineering, ASCE* **2**(4): 204–210.
Kite GW. 1978. Development of a hydrologic model for a Canadian watershed. *Canadian Journal of Civil Engineering* **5**: 126–134.
Kite GW. 1989. Hydrologic modelling with remotely sensed data. In *Proceedings of the 5th Annual Western Snow Conference*, Fort Collins, Colorado, 18–20 April, 1–8.
Kite GW. 1993. Application of a land class hydrological model to climatic change. *Water Resources Research* **29**(7): 2377–2384.
Kite GW, Kouwen N. 1992. Watershed modeling using land classifications. *Water Resources Research* **28**(12): 3193–3200.
Kite GW, Dalton A, Dion K. 1994. Simulation of streamflow in a macroscale watershed using general circulation model data. *Water Resources Research* **30**(5): 1547–1559.
Laramie RL, Schaake JC Jr. 1972. Simulation of the continuous snowmelt process. (ed.); Report 143, Ralph M. Parsons Laboratory, Massachusetts Institute of Technology: Cambridge, MA.
Lee DT, Schactor BJ. 1980. Two algorithms for constructing a Delauney triangulation. *International Journal of Computing and Information Science* **9**(3): 219–242.
Marsh P, Woo MK. 1979. Annual water balance of small high arctic basins. In *Proceedings, Canadian Hydrology Symposium: 79*. Vancouver, British Columbia, Associate Committee on Hydrology, National Research Council of Canada: Ottawa, Ontario; 536–546.
Martinec J, Rango A. 1989. Merits of statistical criteria for the performance of hydrologic models. *Water Resources Bulletin* **25**(2): 412–432.

McNamara JP. 1997. A nested watershed study in the Kuparuk River basin, Arctic Alaska: streamflow, scaling, and drainage basin structure. PhD dissertation, University of Alaska, Fairbanks.
McNamara JP, Kane DL, Hinzman LD. 1997. Hydrograph separations in an arctic watershed using mixing model and graphical techniques. *Water Resources Research* **33**(7): 1707–1719.
McNamara JP, Kane DL, Hinzman LD. 1998. An analysis of streamflow hydrology in the Kuparuk River Basin, Arctic Alaska: a nested watershed approach. *Journal of Hydrology* **206**: 39–57.
Mendez J, Hinzman LD, Kane DL. 1998. Evapotranspiration from a wetland complex on the arctic coastal plain of Alaska. *Nordic Hydrology* **29**(4/5): 303–330.
Moore RD. 1983. On the use of bulk aerodynamic formulae over melting snow. *Nordic Hydrology* **14**(4): 193–206.
Palacios O, Cuevas B. 1986. Automated river course, ridge and basin delineation from digital elevation data. *Journal of Hydrology* **86**: 299–314.
Paniconi C, Wood EF. 1993. A detailed model for simulation of catchment scale subsurface hydrologic processes. *Water Resources Research* **29**(6): 1601–1620.
Petrie G, Kennie TJM. 1987. Terrain modeling in surveying and civil engineering. *Computer Aided Design* **19**(4): 171–187.
Price AG, Dunne T. 1976. Energy balance computations of snowmelt in a subarctic area. *Water Resources Research* **12**(4): 686–694.
Priestley CHB, Taylor TJ. 1972. On the assessment of surface heat flux and evaporation using large-scale parameters. *Monthly Weather Review* **100**: 81–92.
Roots EF. 1989. Climate change: high-latitude regions. *Climate Change* **15**: 223–253.
Rouse WR, Stewart RB. 1972. A simple model for determining the evaporation from high latitude upland sites. *Journal of Applied Meteorology* **11**: 1063–1070.
Rouse WR, Mills PF, Stewart RB. 1977. Evaporation in high latitudes. *Water Resources Research* **13**(6): 909–914.
Rouse WR, Douglas MSV, Hecky RE, Hershey AE, Kling GW, Lesack L, Marsh P, McDonald M, Nicholson BJ, Roulet NT, Smol JP. 1997. Effects of climate change on the freshwaters of Arctic and Subarctic North America. *Hydrological Processes* **11**: 873–902.
Silfer AT, Kinn GJ, Hassett JM. 1987. A geographic information system utilizing the triangulated irregular network as a basis for hydrologic modeling. In *Proceedings of Eighth International Symposium on Computer-assisted Cartography*, Chrisman NR (ed.); Maryland, Baltimore; 29 March–3 April. 129–136.
Stewart RB, Rouse WR. 1976. Simple models for calculating evaporation from dry and wet tundra surfaces. *Arctic and Alpine Research* **8**(3): 263–274.
van Everdingen RO. 1987. The importance of permafrost in the hydrological regime. In *Canadian Aquatic Resources*, Healey MC, Wallace RR (eds); (215). Canadian Bulletin of Fisheries and Aquatic Science: 243–276.
Walker MD, Walker DA, Everett KR. 1989. Wetland soils and vegetation, Arctic foothills, Alaska. *US Department of the Interior Biological Report* **89**(7): 89 pp.
Weller G, Holmgren B. 1974. The microclimates of the arctic tundra. *Journal of Applied Meteorology* **13**: 854–862.
Wigmosta MS, Vail LW, Lettenmaier DP. 1994. A distributed hydrology–vegetation model for complex terrain. *Water Resources Research* **30**(6): 1665–1679.
Wolock DM, Price CV. 1994. Effects of digital elevation model map scale and data resolution on a topography-based watershed model terrain. *Water Resources Research* **30**(11): 3041–3052.
Woo MK. 1982. Snow hydrology of the High Arctic. Paper presented at *Western Snow Conference*, Reno, Nevada, 20–23 April.
Woo MK. 1983. Hydrology of a drainage basin in the Canadian High Arctic. *Annals of the Association of American Geographers* **73**(4): 577–596.
Woo MK. 1986. Permafrost hydrology in North America. *Atmosphere-Ocean* **24**(3): 201–234.
Woo MK, Heron R. 1987. Breakup of small rivers in the subarctic. *Canadian Journal of Earth Science* **24**(4): 784–795.
Woo MK, Sauriol J. 1980. Channel development in snow-filled valleys, Resolute, Northwest Territories, Canada. *Geografiska Annaler* **62A**(1–2): 37–56.
Woolhiser DA, Smith RE, Goodrich DC. 1990. *KINEROS, A Kinematic Runoff and Erosion Model: Documentation and User Manual*. ARS-77. Agriculture Research Service, US Department of Agriculture: Washington, DC.

